

Analytical modelling of period spacings across the HR diagram

M. S. Cunha,^{1,2} P. P. Avelino,^{1,2,3} J. Christensen-Dalsgaard,⁴ D. Stello,^{4,5,6} M. Vrad,¹ C. Jiang,⁷ and B. Mosser,⁸.

¹*Instituto de Astrofísica e Ciências do Espaço, Universidade do Porto, CAUP, Rua das Estrelas, PT4150-762 Porto, Portugal*

²*School of Physics and Astronomy, University of Birmingham, Birmingham, B15 2TT, United Kingdom*

³*Departamento de Física e Astronomia, Faculdade de Ciências, Universidade do Porto, Rua do Campo Alegre 687, PT4169-007 Porto, Portugal*

⁴*Stellar Astrophysics Centre, Department of Physics and Astronomy, Aarhus University, Ny Munkegade 120, DK-8000 Aarhus C, Denmark*

⁵*School of Physics, The University of New South Wales, Sydney NSW 2052, Australia*

⁶*Sydney Institute for Astronomy (SIfA), School of Physics, University of Sydney, NSW 2006, Australia*

⁷*School of Physics and Astronomy, Sun Yat-Sen University, Guangzhou, 510275, China*

⁸*LESIA, Observatoire de Paris, PSL Research University, CNRS, Sorbonne Université, Université Paris Diderot, 92195 Meudon, France*

Accepted XXX. Received YYY; in original form ZZZ

ABSTRACT

The characterisation of stellar cores may be accomplished through the modelling of asteroseismic data from stars exhibiting either gravity-mode or mixed-mode pulsations, potentially shedding light on the physical processes responsible for the production, mixing, and segregation of chemical elements. In this work we validate against model data an analytical expression for the period spacing that will facilitate the inference of the properties of stellar cores, including the detection and characterisation of buoyancy glitches (strong chemical gradients). This asymptotically-based analytical expression is tested both in models with and without buoyancy glitches. It does not assume that glitches are small and, consequently, predicts non-sinusoidal glitch-induced period-spacing variations, as often seen in model and real data. We show that the glitch position and width inferred from the fitting of the analytical expression to model data consisting of pure gravity modes are in close agreement (typically better than 7% relative difference) with the properties measured directly from the stellar models. In the case of fitting mixed-mode model data, the same expression is shown to reproduce well the numerical results, when the glitch properties are known a priori. In addition, the fits performed to mixed-mode model data reveal a frequency dependence of the coupling coefficient, q , for a moderate-luminosity red-giant-branch model star. Finally, we find that fitting the analytical expression to the mixed-mode period spacings may provide a way to infer the frequencies of the pure acoustic dipole modes that would exist if no coupling took place between acoustic and gravity waves.

Key words: stars: evolution – stars: interiors – stars: oscillations

1 INTRODUCTION

Stellar oscillations provide a direct probe of the chemical gradients inside stars caused by different physical processes such as nuclear burning, microscopic diffusion, and macroscopic mixing, in, and beyond, the convectively unstable regions (e.g. [Bossini et al. 2015](#); [Constantino et al. 2015](#); [Pedersen et al. 2018](#)). With the advent of space missions with programmes dedicated to the observation of stellar oscillations, such as CoRoT ([Baglin et al. 2006](#)) and Kepler ([Gilliland et al. 2010](#)), the opportunity to use ultra-precise and abundant seismic data to constrain these physical processes has flourished, establishing new challenges also for the understanding of the relation between the details of the stellar structure and the signatures imprinted by these details on the seismic data (e.g. [Hekker & Christensen-Dalsgaard 2017](#), for a recent review). In this con-

text, the study of internal gravity waves and waves of mixed nature are of particular relevance.

Internal gravity waves are observed in intermediate to high mass pulsators, subdwarf B stars, and white dwarfs. In addition, in subgiant and red-giant stars, waves of mixed nature may be observed, which have the properties of a gravity wave in the inner radiative layers and the properties of an acoustic wave in the stellar envelope. The internal gravity waves are maintained by gravity acting on density fluctuations, have frequencies below the buoyancy frequency, and propagate in non-convective regions only. Their propagation speed depends directly on the buoyancy frequency, defined by

$$N^2 = g \left(\frac{1}{\gamma_1} \frac{d \ln p}{dr} - \frac{d \ln p}{dr} \right), \quad (1)$$

where g is the gravitational acceleration, γ_1 is the first adiabatic

exponent, p is the pressure, ρ is the density, and r is the distance from the stellar centre.

Asymptotically, the oscillation periods of eigenmodes of gravity nature (hereafter, g modes) are approximately equally spaced. Consequently, the difference between two modes of the same degree, l , and consecutive radial orders, n , known as the period spacing, ΔP , is approximately constant. This asymptotic value of the period spacing is given by (Tassoul 1980; Aerts et al. 2010),

$$\Delta P_{\text{as}} = \frac{2\pi^2}{\omega_g}, \quad (2)$$

where,

$$\omega_g \equiv \int_{r_1}^{r_2} \frac{LN}{r} dr, \quad (3)$$

$L^2 = l(l+1)$, and r_1 and r_2 are the inner and outer turning points, respectively, that define the propagation cavity of the g mode.

The above assumes a spherically symmetric stellar equilibrium, thus, it neglects the potential impact of rotation on the oscillations. This can be critical, particularly when considering intermediate to high-mass pulsators which typically rotate fast (see, Aerts et al. 2018, for a recent review). We shall keep this assumption throughout the paper. However, given the importance of rotation for pulsators in particular regions of the HR diagramme, that effect shall be considered in a follow-up work.

Sharp variations in the buoyancy frequency inside the g-mode propagation cavity may deflect the oscillation periods from their asymptotic values. This happens when the scale of variation of N is comparable to, or smaller than the local wavelength of the wave. This kind of variations, known as structural (buoyancy) glitches, cause the period spacing to deviate from the constant asymptotic value. These glitches are associated with strong gradients in chemical composition, resulting from a combination of physical processes, such as nuclear burning, diffusion, and mixing, and may be found at different locations, including at some borders, or former borders, of convective regions and in nuclear burning shells.

The impact of a buoyancy glitch on the period spacing depends strongly on the position of the glitch in the propagation cavity of the g mode. That position is best measured in terms of the buoyancy radius¹, defined by

$$\tilde{\omega}_g^r = \int_{r_1}^r \frac{LN}{r} dr, \quad (4)$$

or the buoyancy depth, defined by $\omega_g^r \equiv \omega_g - \tilde{\omega}_g^r$. The closer the glitch is to the middle of the propagation cavity (defined by $\tilde{\omega}_g^r/\omega_g = 0.5$), the shorter is the scale in which the period spacing varies with frequency. For the remaining of this paper, we shall refer to the inner half of the gravity wave propagation cavity as the region where $\tilde{\omega}_g^r/\omega_g < 0.5$ and to the outer half as the region where $\tilde{\omega}_g^r/\omega_g > 0.5$.

In the case of red-giant stars, where pulsations have a mixed nature, the characteristic pulsation frequency spectrum shows signatures of both gravity and acoustic pulsation spectra. Since the oscillations are driven by convection, the oscillation power is modulated by an envelope centred around the frequency of maximum power ν_{max} , that can be scaled from the solar case (Brown 1991; Kjeldsen & Bedding 1995). Moreover, the period spacing follows

approximately the asymptotic expectation for g modes for frequencies significantly different from what would be the frequencies of pure acoustic modes in the star (i.e., eigenmodes of pure acoustic nature, hereafter, p modes). However, close to the pure acoustic frequencies, there is a strong coupling between the oscillation in the inner (g) and outer (p) cavities and the period spacing decreases significantly with respect to the asymptotic value. These dips in the period spacing are approximately equally spaced in frequency, by the large frequency separation, whose first-order asymptotic value is given by (Tassoul 1980; Gough 1993)

$$\Delta \nu_{\text{as}} = \left(2 \int_0^R c^{-1} dr \right)^{-1}, \quad (5)$$

where c is the sound speed.

The impact of buoyancy glitches on the periods of g modes has been theoretically addressed in previous works in the context of the study of white dwarfs and main-sequence intermediate-mass stars (e.g. Brassard et al. 1992; Miglio et al. 2008; Wu et al. 2018). However, no explicit expression for the period spacing variation was presented by these authors, except for the case of the small glitch limit, when the variation is sinusoidal. Likewise, the frequencies of mixed modes in red-giant stars have been modelled by Mosser et al. (2012), based on the asymptotic work by Shibahashi (1979) and Unno et al. (1989). An explicit expression for the period spacing variations was presented in Mosser et al. (2015), but in a form that requires an interpolation procedure. An equivalent formulation was simultaneously presented by Cunha et al. (2015), and again, independently, by Hekker & Christensen-Dalsgaard (2017), that does not require such interpolation. Cunha et al. (2015) have also studied the combined effect of buoyancy glitches and mode coupling in mixed modes, deriving an explicit, asymptotically-based analytical expression for the period spacings where these effects are accounted for. However, in that work the authors addressed only the case of a glitch modelled by a Dirac delta function, which does not reproduce well the variety of glitch shapes that is found in stellar models (potentially also in real data). Moreover, they concentrated on the case of red giants, for which all observed modes are of mixed nature.

In the present work we investigate the impact of structural glitches on the properties of stellar oscillations further, by considering glitches of different shapes and the signatures they introduce both on mixed modes and on pure gravity modes. We stress that our approach does not assume that the glitch is small and, as a consequence, does not lead to sinusoidal period-spacing variations, except in that limit. In addition, we re-visit the asymptotic description for the case when coupling between acoustic and gravity waves occurs, but no glitch is present in the g-mode cavity. In particular, we demonstrate that the analytical expression proposed by Cunha et al. (2015), now extended in the way discussed in the subsequent sections of this paper, reproduces well the period spacings computed from model data and that it can be used to: (1) model the impact of buoyancy glitches on pure g modes in stars where they are observed, e.g., main-sequence intermediate-mass stars, subdwarf B stars, and white dwarfs, (2) model the coupling between the g and p modes in the absence of glitches in red-giant stars, and (3) model the combined effect of the glitches and coupling on red-giant mixed modes. The general analytical expression for the period spacing is presented in Sec. 2. In Secs 3-5 this expression is tested against model data for three different cases, namely, a case of a glitch and no coupling (so, pure g modes), a case of coupling and no glitch (the typical mixed modes), and a case of combined glitch and coupling effects on mixed modes. In Sec. 6 we discuss our results and

¹ We note that in Cunha et al. (2015) we have mentioned that this definition was different from that in Miglio et al. (2008). In fact, their definition is entirely consistent with ours, the only difference being that we opted to include L in our definition, while they do not do so.

conclude. The details of the analytical derivations are provided in Appendix A.

2 GENERAL ANALYTICAL FORMULATION AND MODELS

The starting point for the work presented here is the expression for the relative period spacing, $\Delta P/\Delta P_{\text{as}}$, in the presence of mode coupling and a buoyancy glitch presented by Cunha et al. (2015), according to which,

$$\frac{\Delta P}{\Delta P_{\text{as}}} \approx \frac{1}{1 - (\omega^2/\omega_g) [d\varphi/d\omega + d\Phi/d\omega]}, \quad (6)$$

where we recall that the asymptotic period spacing ΔP_{as} on the left hand side can be expressed in terms of the buoyancy size of the g-mode cavity, ω_g , following Eq. (2). The coupling phase, φ , incorporates the effect of the coupling between p and g modes on the period spacing and is given by equation 34 in Cunha et al. (2015), namely,

$$\varphi = \text{atan} \left[\frac{q}{\tan[(\omega - \omega_{a,n})/\omega_p]} \right], \quad (7)$$

where

$$\omega_p = \left(\int_{r_3}^{r_4} c^{-1} dr \right)^{-1}, \quad (8)$$

r_3 and r_4 are the turning points of the p-mode cavity, and q is the coupling coefficient (Unno et al. 1989; Takata 2016). Also, $\omega_{a,n}$ is the angular frequency of what would be the pure acoustic mode of (pressure) radial order n , in the absence of mode coupling. The glitch phase, Φ , incorporates the effect of the structural buoyancy glitch. Both phases are frequency dependent. Moreover, in the most general case, the glitch phase Φ depends on the coupling phase φ . This is because the impact of the structural glitch on the oscillation period depends on the phase of the wave at the glitch position and that phase, in turn, may depend on the mode coupling. We further note, from inspection of Eqs (8) and (5), that the quantity ω_p is related to the model asymptotic large frequency separation by $\omega_p \approx 2\Delta\nu_{\text{as}}$, with the restriction that the left-hand side is never smaller than the right-hand side term. Moreover, while ω_p may depend on frequency, through a possible frequency dependence of the turning points, $\Delta\nu_{\text{as}}$ is fully defined by the equilibrium model, hence, is, by definition, frequency independent.

Analytical expressions for the coupling and glitch phases were presented in Cunha et al. (2015) for the case of a glitch modelled by a Dirac delta function located in the outer half of the g-mode cavity. Here we shall present, in addition, formulations for the cases of glitches modelled either by a step function or by a gaussian-like function, which describe more adequately the types of structural variations that are seen in the stellar models considered in this work.

In the absence of a structural glitch, $\Phi = 0$. Then, eq. (6) reduces to,

$$\frac{\Delta P}{\Delta P_{\text{as}}} \approx \frac{1}{1 - (\omega^2/\omega_g) (d\varphi/d\omega)} \equiv \zeta(\omega), \quad (9)$$

an expression that was first presented in Christensen-Dalsgaard (2012), with the explicit form of φ given later by Cunha et al. (2015) (cf. Eq. (7)). In Mosser et al. (2015) this relative bunched period spacing was identified with the function $\zeta(\omega)$ defined by Deheuvels et al. (2015) (following on the work by Goupil et al.

(2013)) in the context of the study of mixed-mode rotational splittings. The frequency position of the acoustic resonances, characterized by an abrupt decrease of the period spacing, corresponds to the minima of the function ζ , and, in turn, to the maxima of $-d\varphi/d\omega$. We shall see, in Sec. 4, that the analytical expression for the relative period spacing presented by Cunha et al. (2015) for the case of coupling and no glitch is equivalent to the function $\zeta(\omega)$, but that it is written in such a way that it is much easier to fit to real data than the version presented by Deheuvels et al. (2015).

It is important to note that the impacts on the period spacing from the mode coupling and from a structural glitch are, generally, not additive. When the glitch effect is small, meaning

$$\left| 1 - \frac{\omega^2}{\omega_g} \frac{d\varphi}{d\omega} \right| \gg \left| \frac{\omega^2}{\omega_g} \frac{d\Phi}{d\omega} \right|, \quad (10)$$

eq. (6) can be approximated by,

$$\frac{\Delta P}{\Delta P_{\text{as}}} \approx \zeta(\omega) + \frac{\omega^2}{\omega_g} \frac{d\Phi}{d\omega}. \quad (11)$$

In this limit case (eq. (11)), the relative period-spacing variation is found to be similar to that presented by Mosser et al. (2015) (their equation 28). However, even in this case there is an important difference between the two results that is worth noting: in eq. (11) the glitch term (second term on the right hand side (rhs)) generally depends on the coupling term, through the dependence of the glitch phase Φ on the coupling phase φ , while that fact was not considered in the work of Mosser et al. (2015). As briefly discussed by Cunha et al. (2015), the fact that Φ generally depends on φ has significant implications for the combined period-spacing modulation at the acoustic resonances, requiring that the two effects are modelled simultaneously, rather than sequentially.

In this work, stellar models will be used to test the analytical expression given by eq. (6) in its various forms described in detail in Secs 3-5. The models, whose global properties are summarised in Table 1, are computed with the evolution code ASTEC (Christensen-Dalsgaard 2008a) and the corresponding pulsation frequencies are computed with the adiabatic pulsation code ADIPLS (Christensen-Dalsgaard 2008b). For the study of the glitch effect on the periods of pure gravity waves we consider a main-sequence stellar model with a mass $M = 6M_{\odot}$ (Sec. 3) and a $1M_{\odot}$ red-giant-branch (RGB) model located at the luminosity bump (the same as Model 1a in Cunha et al. 2015). For the latter we used the ASTER code² to compute the frequencies of what would be the pure g modes if no coupling existed, by artificially disregarding the p-mode cavity, as explained in Cunha et al. (2015) (their section 3.2.3). The effect of the mode coupling in the absence of structural glitches is tested on a $1M_{\odot}$ RGB stellar model with a luminosity that is lower than the luminosity bump (Sec. 4). Finally, the combined effect of mode coupling and a buoyancy glitch is tested on the $1M_{\odot}$ RGB model located at the luminosity bump (Sec. 5), using the mixed-mode frequencies computed with ADIPLS. The choice of this latter RGB model is motivated by the fact that a clear buoyancy glitch is found at that luminosity. Thus, even if mixed modes may be harder to detect observationally in such high-luminosity RGBs (Mosser et al. 2018), the analytical expression is best validated in such a clear case.

² The ASTER code computes the solutions to the adiabatic pulsation equations under the Cowling approximation considering only the g modes. This is done by taking the local radial wavenumber K to be defined by the relation $K^2 = -(L^2/r^2)(1 - N^2/\omega^2)$

Table 1. Properties of the stellar models considered in this work. The frequency of maximum power for the lower luminosity and higher luminosity RGB models are, respectively, $\nu_{\max}=105 \mu\text{Hz}$ and $\nu_{\max}=40 \mu\text{Hz}$

Model	Mass (M_{\odot})	Radius (R_{\odot})	Effective Temp. (K)	Luminosity (L_{\odot})	Age (Gyr)
Main sequence	6.0	3.5	18661	1328	0.0236
RGB-1 (no core glitch)	1.0	5.8	4624	14.0	11.37
RGB-2 (core glitch)	1.0	9.7	4438	32.7	11.45

3 BUOYANCY GLITCH EFFECT ON PURE GRAVITY WAVES

The impact of buoyancy glitches on pure gravity waves has been addressed through asymptotic analysis in previous theoretical works related to white dwarfs (Brassard et al. 1992) and relatively massive main-sequence stars (Miglio et al. 2008). In both cases the glitch was assumed to be well described by a step function and no explicit expression for the period-spacing modulation was presented, except in the limit case of small glitches. In Cunha et al. (2015) an explicit expression for the period-spacing modulation was provided for the effect of a glitch on pure gravity waves, but only for the case of a glitch modelled by a Dirac delta function³. Since that work concerned only red giant stars, the analytical expression was tested on models by computing the pulsation equations with modified boundary conditions that assumed that no p modes were present, to avoid the effect of mode coupling. It was found that, except for the amplitude dependence on frequency, the analytical expression provided a good fit to the numerical results. The mismatch between the frequency dependences of the analytical and numerical amplitudes found by the authors is explained by the fact that in the numerical model the glitch presented a finite width, which was not accounted for when modelling it with a Dirac delta function. To overcome that limitation, here we model again the glitch seen in that RGB model (Model 1a in Cunha et al. 2015) but using, instead, a Gaussian-like function. Moreover, for the case of the main-sequence intermediate-mass model, the glitch will be modelled with a step-like function, as detailed below.

The bottom panels of Fig. 1 show the buoyancy frequency around the position of the glitch for the two models considered in this section, as a function of the relative distance from the centre of the star, r/R , where R is the stellar radius. In the $6 M_{\odot}$, main-sequence stellar model, the buoyancy frequency (Fig. 1 b) drops abruptly at $r^*/R = 0.17$, from the plateau resulting from the steep slope in the hydrogen profile outside the retracting convective core (Fig. 1 a). We note that no smoothing of the composition profile was considered during the evolution of this model. The drop in the buoyancy frequency can be modelled by the discontinuous function,

$$N = \begin{cases} N_{\text{in}} & \text{for } r < r^* \\ N_{\text{out}} & \text{for } r > r^* \end{cases}, \quad (12)$$

with N varying by $\Delta N = N_{\text{in}}|_{r \rightarrow r^*_-} - N_{\text{out}}|_{r \rightarrow r^*_+}$ at $r = r^*$. The glitch is thus characterised by two parameters, namely, the relative step amplitude $A_{\text{st}} = [N_{\text{in}}/N_{\text{out}}]_{r^*} - 1$, and the position, r^* .

In the case of the $1 M_{\odot}$ red-giant model, the buoyancy frequency (Fig. 1 d) shows a hump at $r^*/R = 0.0216$. This hump results from the strong chemical gradient generated at the time of the

first dredge-up and left behind by the retreating convective envelope (Fig. 1 c). Here, numerical diffusion associated to the treatment of the mesh in the stellar evolution code leads to a smoother composition profile, hence also to a broader feature in the buoyancy frequency. We model this glitch using a Gaussian-like function by defining,

$$N = N_0 \left[1 + \frac{A_G}{\sqrt{2\pi}\Delta_g} \exp\left(-\frac{(\omega_g^r - \omega_g^*)^2}{2\Delta_g^2}\right) \right], \quad (13)$$

where N_0 is the glitch-free buoyancy frequency. In this case, the glitch is characterised by three parameters, the constants A_G and Δ_g , which measure, respectively, the amplitude and width of the glitch, and the glitch position r^* , which enters the buoyancy depth at the glitch position, $\omega_g^* = \int_{r^*}^{r_2} (LN/r) dr$. This is in contrast to the model assumed in Cunha et al. (2015), where the glitch was characterised by two parameters only, namely, the amplitude A_g and the position r^* .

The derivation of the eigenvalue condition in the presence of a glitch that leads to the definition of the phase Φ for each case described above is carried out in a way similar to that presented in Cunha et al. (2015) for the case of a glitch modelled by a Dirac delta function. The details are presented in Appendix A. For each glitch considered, we differentiate the glitch phase (given by Eq. (A9) for the step-like glitch and by Eq. (A18) for the Gaussian-like glitch), introduce it into Eq. (6), and take $d\phi/dr = 0$ (in accordance with the no mode coupling assumption made in this section), to obtain the corresponding period spacing.

For a glitch modelled by a step function and located in the inner half of the cavity (as in the main-sequence model considered here) it follows that⁴

$$\frac{\Delta P}{\Delta P_{\text{as}}} \approx \left[1 - \frac{\tilde{\omega}_g^*}{\omega_g} \frac{-A_{\text{st}} \sin \tilde{\beta}_1 + A_{\text{st}}^2 \cos^2 \tilde{\beta}_2}{(1 + A_{\text{st}} \cos^2 \tilde{\beta}_2)^2 + (0.5 A_{\text{st}} \cos \tilde{\beta}_1)^2} \right]^{-1}, \quad (14)$$

where $\tilde{\beta}_1 = 2\tilde{\omega}_g^*/\omega + 2\delta$ and $\tilde{\beta}_2 = \tilde{\omega}_g^*/\omega + \pi/4 + \delta$. Here, quantities marked with a superscript $*$ refer to values taken at $r = r^*$ and δ is a phase related to the details of the mode reflection near the turning points of the propagation cavity (see Appendix A for details).

For the glitch modelled by a Gaussian-like function the derivation of the eigenvalue condition is not as straightforward as for the cases of glitches modelled by a Dirac delta or a step function. The reason is that for the Gaussian-like glitch the derivation requires knowledge of the eigenfunction inside the glitch. As the asymptotic approximation breaks down when the background varies on scales comparable with or smaller than the local wavelength, the asymptotic solution is unlikely to provide an adequate description of the eigenfunction inside the glitch. For a small enough glitch, this problem can be overcome by making use of the variational properties of

³ We note that in that paper there is a typo in equation (25): a minus sign should have preceded the expression for \mathcal{F}_G . The same sign is missing in the second term on the right hand side of equation (39) of the same paper. Nevertheless, all results presented in that work have considered the correct sign and are, therefore, correct.

⁴ The signature on the period spacing from a step-like glitch depends on the side of the cavity where it is located. Deriving the expression for the case of a glitch located in the outer half of the cavity is straightforward following the same steps as in Appendix A.

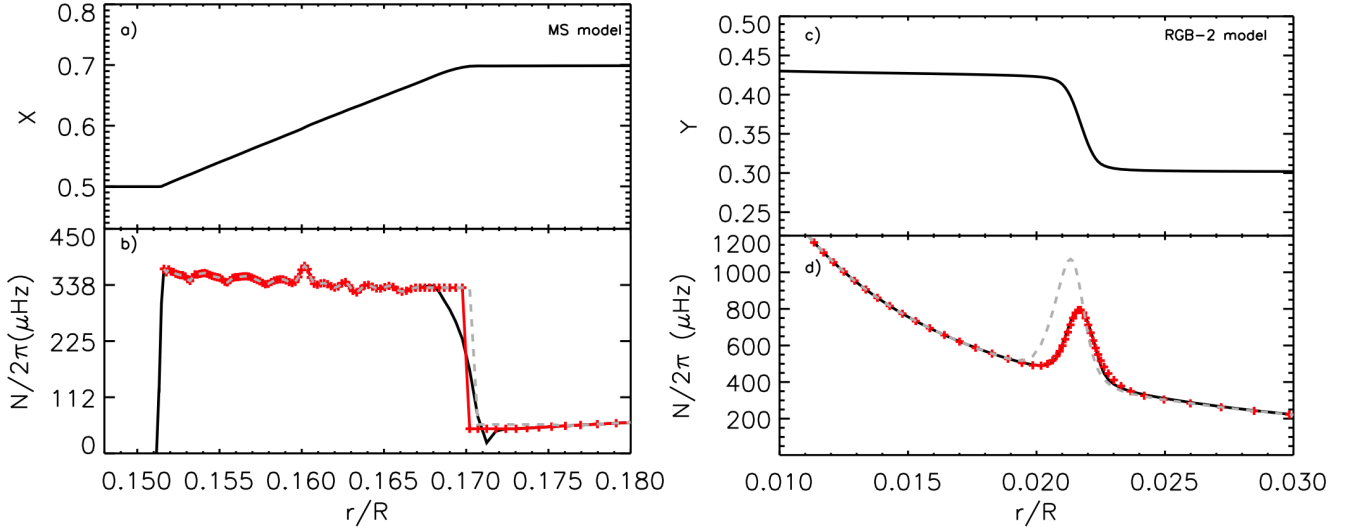


Figure 1. Hydrogen profile (panel a) and buoyancy frequency (panel b) for the $6M_{\odot}$ main-sequence model and helium profile (panel c) and buoyancy frequency (panel d) for the RGB model. The figures show the regions where the glitches are located in these models. The black curves show the results from ASTEC while the red crosses show the models described by Eqs (12) (panel b) and (13) (panel d) used to derive the analytical expressions for the relative period-spacing variation. The grey, dashed lines in the two bottom panels show the buoyancy frequency recovered from the same models when adopting the parameters inferred from the fit of the analytical expressions to the numerical period spacings.

Table 2. Parameters derived from the fit of the analytical expression for the step-like glitch (Eq. (14)) to the period spacing derived from ADIPLS for the main-sequence model. Their distributions are shown in Fig. 2. The values shown correspond to the median of the distributions and the 68% confidence intervals. For comparison, the values of the glitch parameters estimated directly from the buoyancy frequency obtained with ASTEC are also shown. The glitches reconstructed from the inferred and estimated parameters are compared in Fig. 1 b.

	ΔP_{as} (s)	A_{st}	$\tilde{\omega}_{\text{g}}^*$ (10^{-6} rad/s)	δ
Fit	8472^{+50}_{-50}	$4.74^{+0.44}_{-0.39}$	$351.61^{+0.73}_{-0.72}$	$0.602^{+0.019}_{-0.019}$
Estimated	—	5.3	349	—

the solutions that allow us to derive the perturbation to the oscillation periods without explicitly taking into account the perturbation to the eigenfunctions. However, for a glitch such as the one considered here, that option is not available and proceeding with the derivation of the eigenvalue condition and glitch phase requires a somewhat arbitrary choice for the description of the eigenfunction inside the glitch. We have considered two different options for that choice that we discuss in detail in Appendix A. We have tested both cases against the limit of a small glitch modelled by a Gaussian-like function, which can be derived without explicit knowledge of the wave solution. Both cases reproduce the functional form derived in the small-glitch limit, but with a frequency attenuation of the glitch signature that differs from that found in the limit case. In the limit of a small glitch, the perturbation to the periods derived from the variational principle varies exponentially as $\exp(-2\Delta_{\text{g}}^2\omega^{-2})$, whereas the derivation made in Appendix A, which takes the eigenfunction inside the glitch explicitly into account, predicts that the perturbation to the periods varies as $\exp(-0.5\Delta_{\text{g}}^2\omega^{-2})$. Clearly, the expression for a glitch of arbitrary amplitude must reproduce the expression valid in the limit of a small glitch, so it is reasonable to conclude that the difference found results from the inadequate modelling of the eigenfunction inside the glitch. Acknowledging that the very nature of the asymptotic analysis used in our derivation precludes us from improving it, we have changed the factor in

the exponential function to insure that the analytical expression representing the perturbation induced by a glitch of arbitrary strength satisfies the result found in the small-glitch limit, and then tested the modified analytical expression against numerical results. The results from these tests, detailed in Appendix A, support the change in the factor introduced in the exponential function, indicating that such change is necessary also when the glitch is strong. With the correction mentioned above, both analytical expressions derived in the Appendix A provide an adequate fit to the numerical results, although significantly different amplitudes are recovered from the two fits. Here we discuss the analytical expression that was found to perform best against the numerical results, leaving the detailed comparison with the other case to Appendix A.

Considering a glitch located in the outer half of the cavity (as in the case of the RGB model considered here) it follows that the period spacing for the Gaussian-like glitch is given by⁵

$$\frac{\Delta P}{\Delta P_{\text{as}}} \approx \quad (15)$$

⁵ For a glitch located on the inner half of the cavity the expression would be the same, but with ω_{g}^* replaced by $\tilde{\omega}_{\text{g}}^*$.

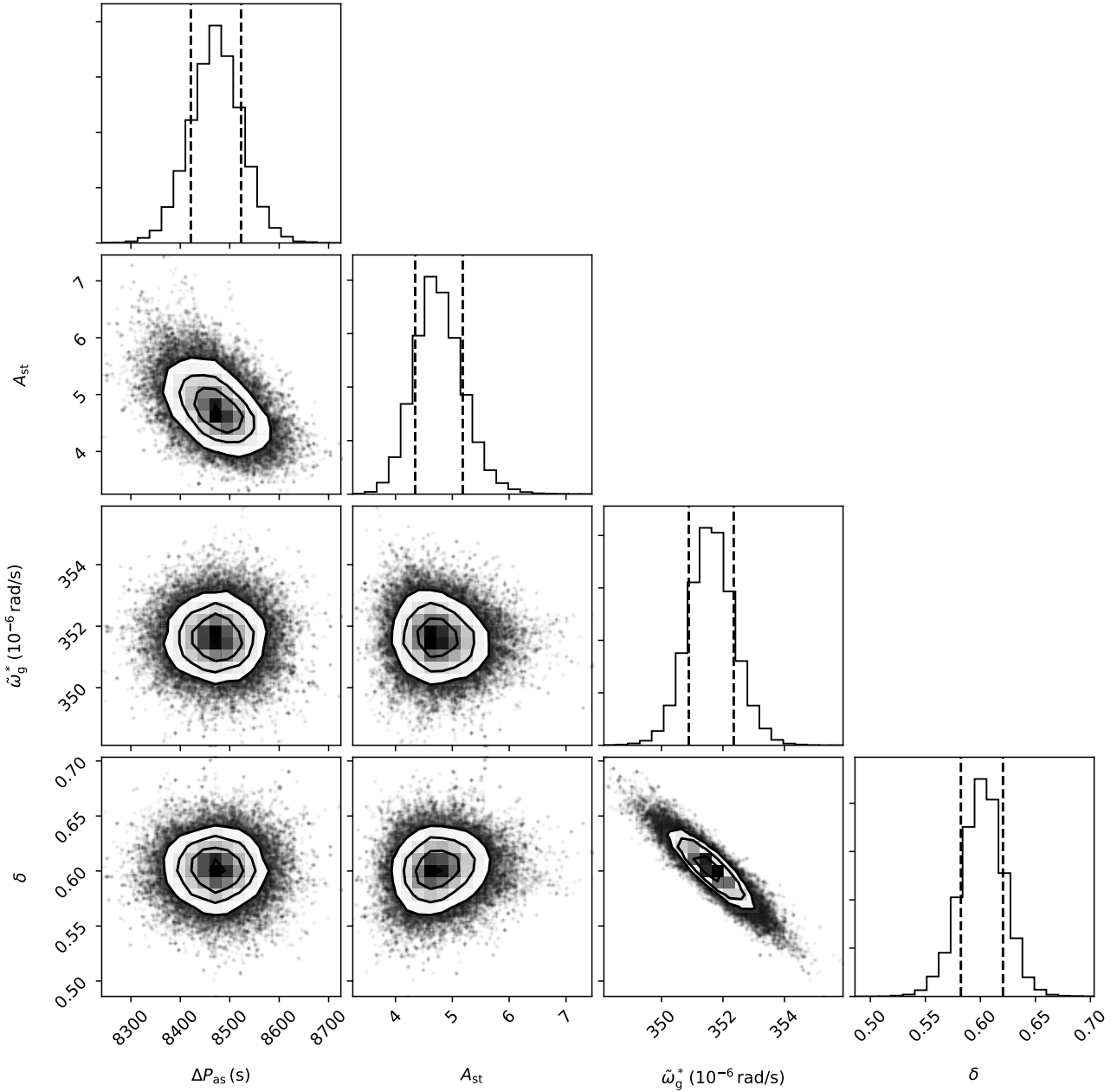


Figure 2. Marginalised distributions for the parameters considered in the fit of the rhs of Eq. (14) to the period spacing derived from ADIPLS for the main-sequence model.

$$\left[1 + A_G f_{\omega}^{\Delta_g} \frac{\omega_g^*}{\omega_g} \frac{\left[\cos \beta_1 + \left(\omega / \omega_g^* (1 - 4\Delta_g^2 / \omega^2) - A_G f_{\omega}^{\Delta_g} \right) \sin^2 \beta_2 \right]}{(1 - 0.5 A_G f_{\omega}^{\Delta_g} \cos \beta_1)^2 + (A_G f_{\omega}^{\Delta_g} \sin^2 \beta_2)^2} \right]^{-1}$$

where we introduced the frequency-dependent function $f_{\omega}^{\Delta_g} = \omega^{-1} e^{-2\Delta_g^2 \omega^{-2}}$. Moreover, here $\beta_1 = 2\omega_g^* / \omega + 2\delta$ and $\beta_2 = \omega_g^* / \omega + \pi/4 + \delta$.

The analytical expressions for the relative period spacing presented above will be useful for fitting real data and extracting information about the structural variations. Here we test their suitability based on fits to model data in the following. In this context

it is important to emphasise that in addition to the glitch parameters discussed before (two in the case of the step model and three in the case of the Gaussian model) these expressions contain also one global seismic parameter, namely, $\Delta P_{as} = 2\pi^2 / \omega_g$, and the phase parameter, δ . Tables 2 and 3 summarise the values inferred for the parameters from the fitting of the analytical expressions to the model data, for the two glitches considered. The inferred glitch parameters are to be compared with their estimated values obtained directly from the buoyancy profiles (red crosses in Fig. 1 b,d).

The rhs of equation Eq. (14) was fitted to the period spacings computed from the eigenfrequencies obtained with the pulsation

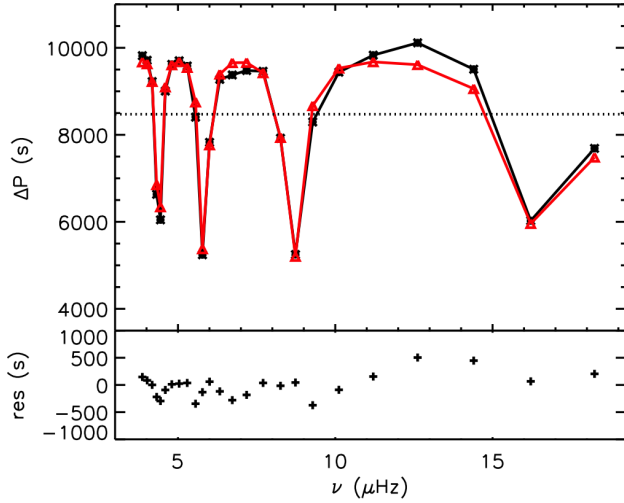


Figure 3. Top panel: comparison between the period spacing derived from ADIPLS (black line and asterisks) for the main sequence model and that obtained from Eq. (14) with the most likely parameters from our fit, performed in the frequency range shown in the figure (red line and triangles). Bottom panel: the residuals (‘ADIPLS period spacing’ – ‘analytical period spacing’)

code ADIPLS for the main sequence model, ΔP_{ADIPLS} , using the python module *emcee* implementation of the affine-invariant ensemble sampler for Markov chain Monte Carlo (Foreman-Mackey et al. 2013) with the likelihood defined by

$$\mathcal{L} = \frac{1}{\sqrt{2\pi}\sigma} \exp\left(-\frac{1}{2}\chi^2\right), \quad (16)$$

where the uncertainty σ was left as a free parameter and

$$\chi^2 = \sum_i \left(\frac{\Delta P_i - \Delta P_{\text{ADIPLS},i}}{\sigma} \right)^2. \quad (17)$$

The probability density functions obtained for the parameters in the fit are shown in Fig. 2. A comparison of the glitch parameters derived in this way with the values inferred directly from the buoyancy frequency (Table 2) shows a reasonable agreement. While the small differences appear significant, given the errors, they are fully justified by the fact that the step function does not provide an accurate description of the glitch, as seen from Fig. 1 b. In this figure we show, for comparison, the glitch model used to estimate the parameters provided in Table 2 (red crosses) and the glitch recovered from the parameters inferred from the fit to the period spacings (dashed, grey line). The estimated position of the glitch shown in red was taken to be the mid point between the plateaus on the right and left sides of the buoyancy jump. However, given that the jump has a finite extent, the uncertainty associated to this position is more significant than the difference between the estimated and inferred values. Similarly, Fig. 1 b indicates that the difference between the estimated and inferred amplitudes can be accounted for by the deviation of the glitch from a true step function. Figure 3 shows a comparison of the period spacing computed from the ADIPLS results (black) and that obtained from Eq. (14) (red) with the parameters of the most likely model for the fit considered in Fig. 2.

To test the analytical expression for the relative period-spacing variation caused by a Gaussian-like glitch, the rhs of equation Eq. (15) was fitted to the period spacings computed from the eigenfrequencies of pure g modes obtained with the ASTER code for the RGB-2 model (cf. Table 1). The probability density functions

obtained for the parameters entering the fit are shown in Fig. 4. Figure 5 shows a comparison of the period spacing computed from the ASTER results (black) and that obtained from Eq. (15) (red) with the parameters of the most likely model from that fit.

A comparison of the glitch parameters inferred in this way with the values derived directly from the buoyancy frequency (Table 3) shows that the inferred width of the glitch is in agreement with the estimated one. As for the buoyancy depth of the glitch, ω_g^* , the value inferred from the fit differs from that estimated by $\sim 7\%$. This difference is significant, given the small errors, and we have checked that it cannot be explained by an uncertainty in the estimated parameter. In fact, from inspection of Fig. 1 d it seems unlikely that it is related to the modelling of the glitch, which is well represented by Eq. (13). On the other hand, we note that the difference is smaller than the width of the glitch. Given the approximations made in the course of the derivation of the analytical expression, the width of the glitch may, in fact, set a limit to the accuracy with which ω_g^* can be derived through this method. Finally, the amplitude inferred from the fitting is clearly overestimated, indicating that the predictive power of the analytical expression is more limited for this parameter. The buoyancy glitch that results from assuming the parameters inferred from the fitting is shown in grey on Fig. 1 d, for comparison with the glitch seen on the ASTEC model.

An important aspect to note when comparing the signatures on the period spacing of glitches modelled by different functions is that the frequency dependence of the glitch signature’s amplitude (*i.e.* the maximum to minimum period-spacing variation induced by the glitch) is different. For the step-like glitch, we see from Eq. (14) that the amplitude of the glitch signature on the period spacing is determined by the glitch amplitude, A_{st} , and by the glitch location (implicit in $\tilde{\omega}_g^*$) both of which are frequency independent. Thus the signature’s amplitude is also independent of frequency. On the other hand, for the Gaussian-like glitch, we see from Eq. (15) that the amplitude of the glitch signature depends, in addition, on the function $f_{\omega_g^*}^{\Delta_g}$. As a consequence, in this case the amplitude of the glitch signature decreases with decreasing frequency at low frequencies and with increasing frequency at high frequencies. This difference is not so evident in Figs 3 and 5 because the frequency range shown is relatively small, but it is clear when one compares the case of the Gaussian-like glitch and the case of the Dirac delta glitch adopted by Cunha et al. (2015) (see their Fig. 4). In the latter case the amplitude of the glitch signature shows a strong increase with decreasing frequency. That is the reason why the expression for the glitch modelled by a Dirac delta adopted in their work did not reproduce well the signature of the glitch seen in the RGB model. In fact, when the oscillation frequency decreases, the characteristic scale of the gravity wave at the glitch position decreases, and the width of the glitch eventually becomes comparable with the local wavelength. As a consequence, the glitch impact on the wave propagation decreases, leading to a decrease of the amplitude of the glitch effect on the period spacing, as seen in the Gaussian-like case. However, when the glitch is modelled by a Dirac delta function, its width is infinitely small and, therefore, always infinitely smaller than the local wavelength, preventing the above effect from taking place.

Similar differences in the frequency dependence of the glitch signature’s amplitude, according to the glitch model adopted, have been found also in a number of previous works related to both buoyancy and acoustic glitches (e.g. Monteiro et al. 1994; Houdek & Gough 2007; Miglio et al. 2008).

Table 3. Parameters derived from the fit of the analytical expression for the Gaussian-like glitch (Eq. (15)) to the period spacing derived from ASTER for the RGB-2 model (at the luminosity bump). Their distributions are shown in Fig. 4. The values shown correspond to the median of the distributions and the 68% confidence intervals. For comparison, the values of the glitch parameters estimated directly from the buoyancy frequency obtained with ASTEC are also shown. The glitches reconstructed from the inferred and estimated parameters are compared in Fig. 1 d.

	ΔP_{as} (s)	A_G (10^{-6} rad/s)	ω_g^* (10^{-6} rad/s)	Δ_g (10^{-6} rad/s)	δ
Fit	$67.534^{+0.005}_{-0.005}$	607^{+27}_{-25}	$1747.3^{+7.6}_{-7.7}$	$158.5^{+3.4}_{-3.4}$	$-0.872^{+0.034}_{-0.034}$
Estimated	—	380	1632	156	—

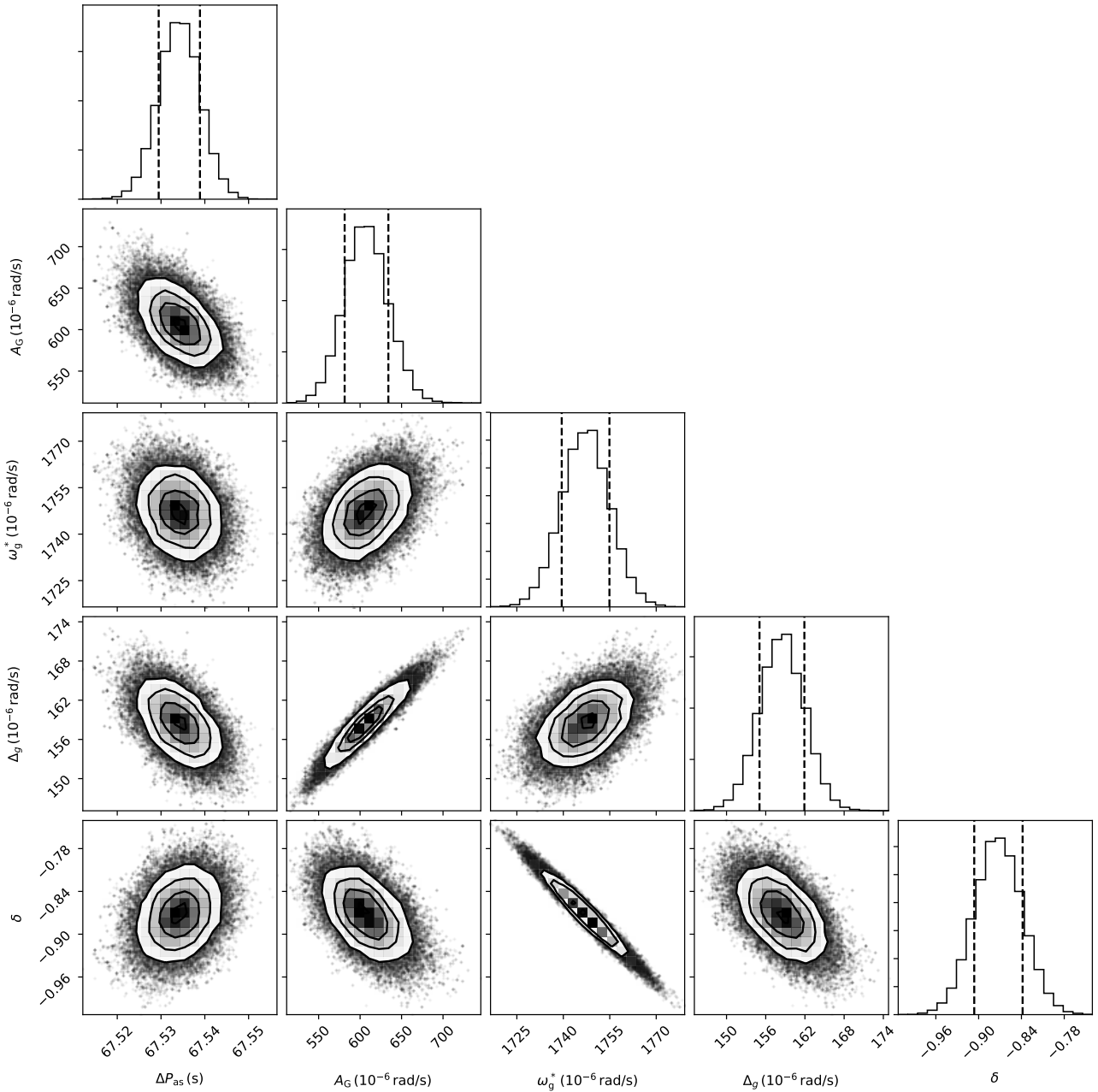


Figure 4. Marginalised distributions for the parameters considered in the fit of the rhs of Eq. (15) to the period spacing derived from ASTER for our RGB-2 model (with a core glitch), when coupling between the p and g modes is ignored.

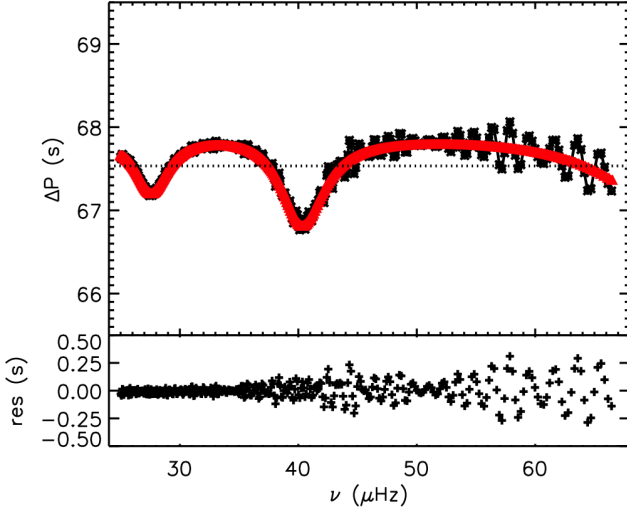


Figure 5. Top panel: comparison between the period spacing derived from ASTER for our RGB-2 model with a core glitch (black line and asterisks), when coupling between the p and g modes is ignored, and that obtained from Eq. (15) with the most likely parameters from our fit, performed in the frequency range shown in the figure (red line and triangles). The short scale variations in the black curve result from rapid variations in the second derivative of the buoyancy frequency at the H-burning shell which are unphysical and, thus, not accounted for in the analytical model. Bottom panel: the residuals (‘ASTER period spacing’ – ‘analytical period spacing’).

4 COUPLING BETWEEN P AND G WAVES IN THE ABSENCE OF GLITCHES

In red giants, when no structural glitches are present, the period spacing deviates from the asymptotic value due to the coupling between acoustic and gravity waves in a manner described by Eq. (9). According to Cunha et al. (2015) in this case we have,

$$\frac{\Delta P}{\Delta P_{\text{as}}} \approx \left[1 + \frac{\omega^2}{\omega_g^2} \frac{q}{\omega_p} \left[\sin^2 \left(\frac{\omega - \omega_{a,n}}{\omega_p} \right) + q^2 \cos^2 \left(\frac{\omega - \omega_{a,n}}{\omega_p} \right) \right]^{-1} \right]^{-1} \quad (18)$$

$$\equiv \zeta(\omega)$$

where the coupling coefficient, q , is considered to be independent of the frequency (a condition that will be re-visited below).

We used the analytical expression provided by Eq. (18) to fit model data following the same approach as in Sec. 3. In Cunha et al. (2015), a series of $1 M_{\odot}$ stellar models obtained from evolution tracks covering the RGB evolution phase was tested for the presence of structural glitches in the core. Signatures of these glitches were found only in models at the luminosity bump. Thus, a model with luminosity below the bump, extracted from that series, was chosen to test Eq. (18) (model RGB-1 in Table 1).

In this case, the parameters to be fitted are the global quantities $\Delta P_{\text{as}} = 2\pi^2/\omega_g$ and $\omega_p \approx 2\Delta\nu_{\text{as}}$, the coupling coefficient, q , and the pure acoustic frequencies $\omega_{a,n}$. However, the asymptotic analysis of the pulsation equations allows us to estimate $\omega_{a,n}$ from the frequencies of radial modes. With this in mind, when fitting Eq. (18) to model data we have considered two different options to obtain $\omega_{a,n}$, both based on the asymptotic expression for the eigenfrequencies (see Appendix B, for details), namely:

1. The frequency $\omega_{a,n}$ is estimated from the frequency of the radial mode with the same radial order, $\omega_{a,n}^0$ through,

$$\omega_{a,n} = \omega_{a,n}^0 + \pi\Delta\nu_0 + \frac{4\pi^2 C}{(\omega_{a,n}^0 + \pi\Delta\nu_0)}, \quad (19)$$

2. The frequency $\omega_{a,n}$ is estimated through the relation,

$$\omega_{a,n} = 2\pi(n+0.5)\Delta\nu_0 + 2\pi G_{a,n} + \frac{4\pi^2 C}{(\omega_{a,n}^0 + \pi\Delta\nu_0)}. \quad (20)$$

In both cases, C is a constant parameter to be fitted and $\Delta\nu_0$ is the average large frequency separation for radial modes in the range of radial orders considered. Moreover, the term $2\pi G_{a,n}$ is obtained by linearly interpolating $\omega_{a,n}^0 - 2\pi n\Delta\nu_0$, at the frequency $\omega_{a,n}^0 + \pi\Delta\nu_0$. By using either of the options above, we require only a single parameter, C , and knowledge of the radial mode frequencies, to express all $\omega_{a,n}$. This reduces the total number of parameters in the fit, and, at the same time, guarantees that the $\omega_{a,n}$ values are related in a way that makes physical sense.

The potential advantage of eq. (20), over eq. (19), is that it accounts for additional frequency dependences of the eigenfrequencies that are common to modes of degree $l = 0$ and $l = 1$, including a possible large-scale frequency variation of the phase that enters the first-order term of the asymptotic expression, as well as variations introduced by a departure from the asymptotic expression, in particular by acoustic glitches in the outer convective envelope. We tested these two formulations on a standard solar model, for which the $l = 1$ modes are not mixed and, therefore, are known a priori. The results of that test confirm that Eq. (20) reproduces the true $l = 1$ frequencies significantly better (the details are discussed in Appendix B).

Figure 6 shows the comparison between the period spacing computed from the ADIPLS results for a glitch-less RGB model and those obtained from Eq. (18) adopting the parameters of the most likely solution found from the fit. The left and right panels differ only in the option adopted for the estimate of $\omega_{a,n}$ (eqs (19) and (20), respectively). While the quality of the fit for option 2 is the better of the two, it is quite clear from Fig. 6 that for both options the analytic formulation fails to reproduce the dips. This is not entirely surprising, because models predict that the coupling coefficient for stars ascending the RGB should be frequency dependent (Jiang & Christensen-Dalsgaard 2014; Hekker et al. 2018). That dependence, which is present for models with $v_{\text{max}} \lesssim 100 \mu\text{Hz}$, results from the fact that the acoustic cavity becomes deeper with increasing frequency while the g-mode cavity barely changes, resulting in a decrease of the width of the evanescent region, with increasing frequency. According to Jiang & Christensen-Dalsgaard (2014), the frequency dependence of q is well represented by a linear function, for models ascending the RGB.

To test the frequency dependence of q , we have performed a third fit to the period spacings obtained from ADIPLS, considering a linear frequency dependent coupling coefficient, defined by

$$q = q_1 [\alpha (v/v_{\text{max}} - 1) + 1], \quad (21)$$

thus replacing the parameter q by the pair of parameters (q_1, α) . Since q enters the definition of the coupling phase φ , its dependence on frequency needs to be taken into account when differentiating φ in Eq. (9). In that case, the analytical expression for the period spacing in the presence of mode coupling, without a buoyancy glitch, previously given by Eq. (18), is replaced by

$$\frac{\Delta P}{\Delta P_{\text{as}}} \approx \left[1 + \frac{\omega^2}{\omega_g^2} \frac{q}{\omega_p} \left[\sin^2 \left(\frac{\omega - \omega_{a,n}}{\omega_p} \right) + q^2 \cos^2 \left(\frac{\omega - \omega_{a,n}}{\omega_p} \right) \right]^{-1} + Q(\omega) \right]^{-1}, \quad (22)$$

where the function $Q(\omega)$ is given by,

$$Q(\omega) = \frac{q_1 \alpha \omega^2}{2\pi v_{\text{max}} \omega_g} \left[q^2 \cot \left(\frac{\omega - \omega_{a,n}}{\omega_p} \right) + \tan \left(\frac{\omega - \omega_{a,n}}{\omega_p} \right) \right]^{-1}. \quad (23)$$

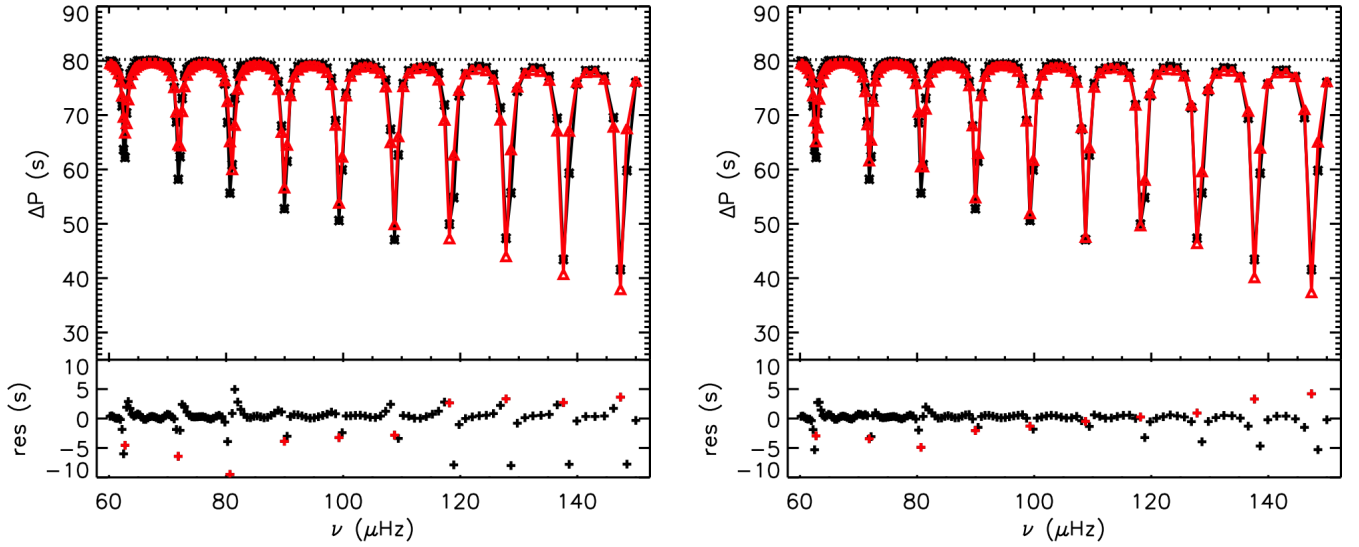


Figure 6. Top panels: comparison between the period spacing derived from ADIPLS for our RGB-1 model (with no core glitch) (black line and asterisks) and that obtained from Eq. (18) with the most likely parameters from our fit, performed in the frequency range shown in the figures (red line and triangles). Left is for $\omega_{a,n}$ estimated through eq. (19) and right is for $\omega_{a,n}$ estimated through eq. (20). Bottom panels: the residuals (‘ADIPLS period spacing’ – ‘analytical period spacing’) for each case. The red symbols mark the residuals at the minima of the ADIPLS period spacing.

Table 4. Parameters derived from the fit of the analytical expression in Eq. (22) to the period spacing derived from ADIPLS for the model RGB-1. Their distributions are shown in Fig. 7. The values shown correspond to the median of the distributions and the 68% confidence intervals. We recall that $\Delta\nu_{\text{as}} \approx \omega_p/2$.

ΔP_{as} (s)	$\omega_p/2$ (μHz)	q_1	C (μHz^2)	α
$80.10^{+0.10}_{-0.09}$	$11.02^{+1.55}_{-1.17}$	$0.128^{+0.015}_{-0.015}$	$19.93^{+0.53}_{-0.53}$	$0.692^{+0.046}_{-0.048}$

The results of the fit when q is considered frequency dependent are shown in Figs 7 and 8. Clearly, the parameter α introduced in association to the frequency dependence of q is well constrained in a region that excludes zero (Fig. 7), confirming that a frequency-independent q does not provide a good fit. The quality of the fit is also found to be substantially better than when q is taken to be constant, a fact that is noticeable when comparing Fig. 8 with Fig. 6. Naturally, the larger the number of radial orders fitted, the more noticeable the frequency dependence becomes. When fitting observational data, with a limited number of radial orders available, one must thus verify whether adding one additional parameter to characterise the frequency dependence of q is a relevant option.

The increase of the depth of the acoustic cavity with frequency, used as an argument to make q frequency dependent, influences also the parameter ω_p , defined by Eq. (8), which, as a result, decreases with frequency. Due to the roles of q and ω_p in Eq. (18), this frequency dependence of ω_p , not accounted for in the previous fit, would emphasise even further the need for a frequency dependence of q . However, according to the work by Jiang & Christensen-Dalsgaard (2014), the frequency dependence of ω_p is generally small and becomes even smaller at the highest frequencies, being well fitted by a second order polynomial. To verify whether this dependence influences the significance found in our previous fit for a frequency dependence of q , we have performed a fourth fit, taking both q and ω_p as frequency dependent, allowing that dependence to go to second order. We found that the parameters characterising the frequency dependence of ω_p were consistent with this parameter being constant, confirming that its frequency

dependence is small. Moreover, the q parameter was confirmed to be well described by a linear dependence on frequency (the second order term being consistent with zero), with an α value consistent with that found in the previous fit, albeit less well constrained, as expected, given the larger number of parameters being fitted.

5 COMBINED EFFECT OF MODE COUPLING AND A BUOYANCY GLITCH

When both mode coupling and a structural glitch in the core are present, the exact form of Eq. (6) depends again on the functional form adopted to model the glitch. In Cunha et al. (2015) the authors presented the expression for the case of a core glitch placed in the outer half of the g-mode cavity, where the glitch was modelled with a Dirac delta function⁶ and the coupling coefficient q was considered to be independent of frequency.

Here, we provide the analytical expression for the case of a glitch in the outer half of the cavity⁷ modelled by the Gaussian-like function discussed in Sec. 3. We thus assure that the functional form adopted for the glitch represents adequately the core glitch seen in the RGB model located at the luminosity bump (model

⁶ We note again that there is a typo in that expression and the reader is advised to see footnote 1 in the present paper for further details.

⁷ In the case of mixed modes, the signature from the Gaussian-like glitch is not invariant with respect to symmetric changes about the center of the g-mode cavity (cf. discussion in Appendix A).

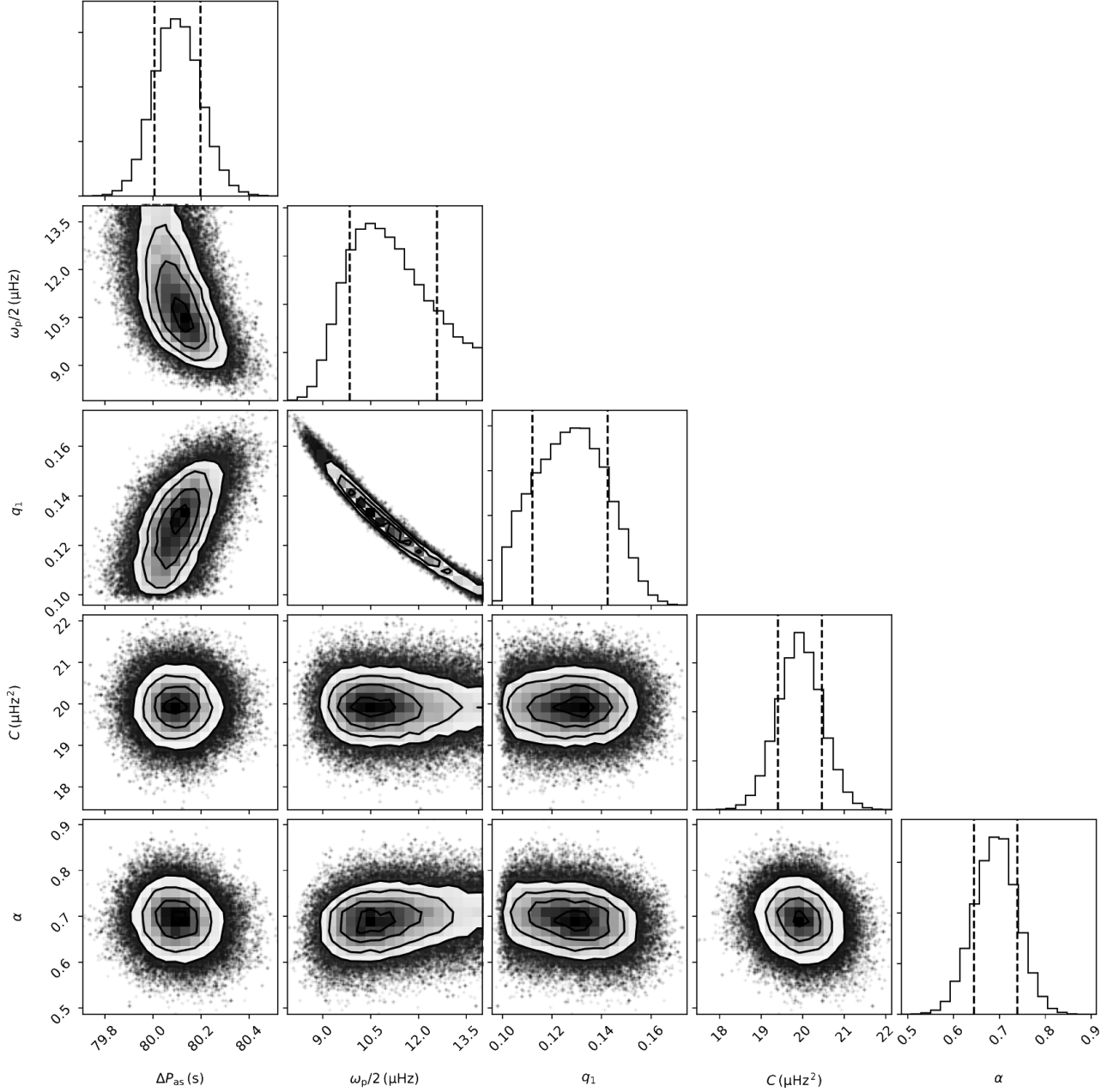


Figure 7. Marginalised distributions for the parameters considered in the fit of the rhs of Eq. (22) to the period spacing derived from ADIPLS for the RGB model below the luminosity bump (model RGB-1, with no glitch), when considering a frequency dependent q according to Eq. (21).

RGB-2), discussed in Sec. 3. In the case of a Gaussian-Like glitch, Eq. (6) can be re-written as (see Appendix A, for details),

$$\frac{\Delta P}{\Delta P_{\text{as}}} \approx [1 - \mathcal{F}_{G,C}]^{-1} \quad (24)$$

where,

$$\mathcal{F}_{G,C} = \frac{\omega^2}{\omega_g} \frac{d\varphi}{d\omega} \left\{ 1 + \frac{A_G f_{\omega_g}^{\Delta_g}}{B^2} [\cos(\beta_{1,\varphi}) - A_G f_{\omega_g}^{\Delta_g} \sin^2(\beta_{2,\varphi})] \right\} \quad (25)$$

$$- \frac{\omega_g^* A_G f_{\omega_g}^{\Delta_g}}{\omega_g B^2} \left\{ \cos(\beta_{1,\varphi}) + \left[\omega / \omega_g^* (1 - 4\Delta_g^2 / \omega^2) - A_G f_{\omega_g}^{\Delta_g} \right] \sin^2(\beta_{2,\varphi}) \right\}$$

and B^2 is given by

$$B^2 = \left[1 - 0.5 A_G f_{\omega_g}^{\Delta_g} \cos(\beta_{1,\varphi}) \right]^2 + \left[A_G f_{\omega_g}^{\Delta_g} \sin^2(\beta_{2,\varphi}) \right]^2. \quad (26)$$

Here, the arguments of the sinusoidal functions are changed with respect to the Gaussian glitch case presented in Sec. 3, now being given by $\beta_{1,\varphi} = \beta_1 + 2\varphi$ and $\beta_{2,\varphi} = \beta_2 + \varphi$, where β_1, β_2 and other glitch-related quantities are defined in that section. This change is a consequence of the dependence of the glitch phase on the coupling

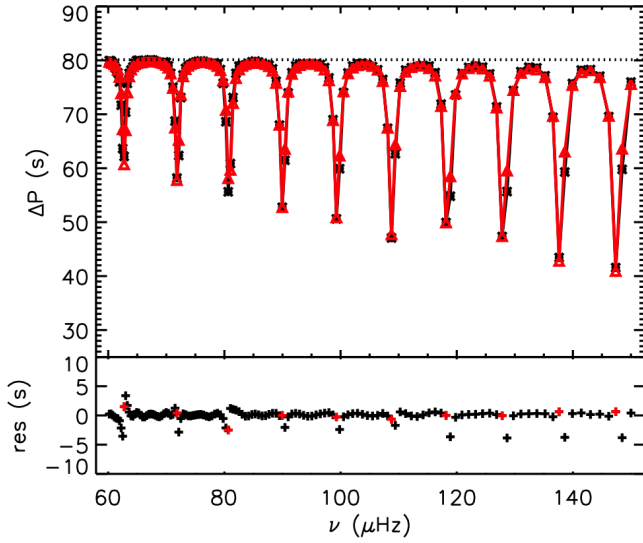


Figure 8. Top panel: Comparison between the period spacing derived from ADIPLS for the RGB-1 model (with no core glitch) (black line and asterisks) and that obtained from Eq. (22) with a frequency dependent q , with the most likely parameters from our fit, performed in the frequency range shown in the figure (red line and triangles). Bottom panel: the residuals (‘ADIPLS period spacing’ – ‘analytical period spacing’). The red symbols mark the residuals at the minima of the ADIPLS period spacing.

phase. Moreover, based on the results of Sec. 4, when testing this analytical expression against model data, q will be taken to depend on the frequency according to Eq. (21). The explicit form of $d\phi/d\omega$ is obtained from the analytical differentiation of Eq. (7).

To test the analytical expression defined by Eqs (24)–(26) we fit it to the period spacings derived from the ADIPLS frequencies for our RGB model located at the luminosity bump (model RGB-2), following the same approach as in Sec. 3. We start by fixing the glitch parameters, A_G , Δ_g , ω_g^* , and δ at the values derived in Sec. 3 and adopt Eq. (20) to describe the pure acoustic frequencies $\omega_{a,n}$. The problem thus involves fitting five parameters: two characterising the global seismic properties (ω_p and ΔP_{as}), two other characterising the mode coupling (q_1 and α), and one characterising the relation between the frequencies of pure acoustic modes (C).

The results of the fit are shown in Fig. 9, left panel, where it can readily be noticed that the model, with the parameters from the best fit, fails to reproduce adequately the ADIPLS results near some of the coupling dips. We note, however, that in the model under consideration the variation of the period spacing near the pure acoustic frequencies is extremely large. Hence, the accuracy to which one derives the $\omega_{a,n}$ values can be of importance to the quality of the fit. In particular, it is important to establish whether the failure to properly fit the model period spacings is a consequence of the inadequacy of the analytical expression used in the fit, or if it results, instead, from the insufficient accuracy of the pure acoustic frequencies estimated from Eq. (20).

In the case of the Sun, discussed in Appendix B, we find that some frequency-dependent residuals remain when the $l = 1$ model frequencies are compared with the estimates obtained from Eqs. (19) and (20). To test the impact of small variations of $\omega_{a,n}$ on the fit, we performed the fit on RGB-2 model again, under two different conditions: i) estimating $\omega_{a,n}$ from Eq. (19) and, ii) letting the $\omega_{a,n}$ values be independent free parameters. In the first case we found that the quality of the fit got worse compared to Fig. 9 (left

panel), reflecting that the estimates of the pure acoustic frequencies worsened, as expected from the results for the solar case. On the other hand, the fit was much improved when these frequencies were let free, as seen from the inspection of Fig. 9, right panel.

The significant improvement in the fit observed in the last case discussed above is not a surprise in itself, given the increase in the number of free parameters. It is, thus, important to assess whether the set of $\omega_{a,n}$ retrieved from the fit in this case makes physical sense, or, rather, is simply a combination of unrelated departures from the previous estimates that results from the fitting procedure attempting to correct a possible inadequacy of the analytical representation of the period spacing. To clarify this matter we computed the differences between the frequencies $\omega_{a,n}$ obtained from the fit where these have been left as free parameters and those obtained from Eqs (19) and (20) with values of C derived from the corresponding fits. The comparison is shown in Fig. 10 for a sample of 30 best fitted models (with similar likelihood). The comparison of the results in Fig. 10 with those found for the solar model S (Fig. B1), is very encouraging. In particular, the difference between the freely-determined $\omega_{a,n}$ and the $\omega_{a,n}$ estimated from Eq. (19) shows a trend with frequency that resembles that found for the solar model when the frequencies estimated by Eq. (19) are subtracted from the exact $l = 1$ model frequencies. This is particularly significant, because the estimate of $\omega_{a,n}$ through Eq. (19) does not depend on any interpolation procedure whose adequacy may be different for the Sun and for a red-giant model. We note that the differences shown in Fig. 10 (scaled to the model large frequency separation) for the RGB model are about one order of magnitude larger than those found for the solar model, for the same range of radial orders around ν_{\max} . This is true both for the differences illustrated by the curve in grey and for those illustrated by the curve in red. That can be understood from the fact that both the frequency signature of acoustic glitches associated with the helium second ionization and the large-scale frequency variation associated to surface effects are, after scaling by the large separation, about one order of magnitude larger in the RGB model compared to the solar model (e.g. Broomhall et al. 2014; Houdek & Gough 2007). In addition, in the solar model the signature of the glitches on the frequencies is better resolved, because of the denser acoustic frequency spectrum. These two facts explain that the difference between the true frequencies and the estimated ones is more significant in the RGB model. Given the evidence above, we are confident that the estimates of the $\omega_{a,n}$ derived from the fit of the analytical expression defined by Eqs (24)–(26) to the period spacing of this luminous RGB model, are the best of the three possible estimates considered here. So, we trust that having $\omega_{a,n}$ free when fitting such a luminous RGB star is the best option in the present case.

Following on the results discussed above, we attempted to perform the same fits, with the different options for the pure acoustic frequencies, by considering the glitch parameters to be free. Unfortunately, none of the options considered produced reasonable constraints to the glitch parameters. This is because the χ^2 minimisation is heavily influenced by small departures between the analytical expression and the model data at the frequencies around the acoustic dips, where the period spacing varies abruptly. Hence, the quality of the fit is not sufficiently sensitive to the glitch parameters in this case. As an example, we find that fits corresponding to a no-glitch solution (with a flat period spacing everywhere except around the coupling dips) can have a similar χ^2 as that shown in Fig. 9, right panel. This experience points towards the need to adopt a different strategy, perhaps not based on a global χ^2 criteria, to constrain the parameters of the glitch from the analytical expression presented in

Eqs (24)-(26). However, the results found when fixing the parameters of the glitch do confirm that the proposed analytical expression provides a good representation of the model period spacing in the presence of a core structural glitch and mode coupling.

6 CONCLUSIONS

In this work we have tested an analytical representation of the dipole mode period spacing derived from asymptotic analysis against model data. The analytical expression is relevant for the modelling of stars exhibiting pure gravity modes as well as stars exhibiting mixed modes. The impact of different types of structural glitches that may be present in the cores of the stars has been fully accounted for, as has the coupling between p and g modes, when present. Rotation effects have not been considered.

With the exception of the amplitude in one of the cases considered, our results show that the buoyancy-glitch parameters can be adequately recovered by fitting the proposed analytical expression to model data consisting of pure gravity modes. We stress that unlike in previous works, the analytical expression tested here is valid also when the glitch is not small and, consequently, when the glitch-induced period spacing variations are not sinusoidal. This is important because when the glitch is not small the period spacing is asymmetric with respect to the asymptotic value and fitting it with a sinusoidal function, such as that predicted in the small glitch limit, may lead to a biased estimation of the asymptotic period spacing, as well as of the glitch parameters.

For the case of pure gravity modes, the relative differences between the glitch parameters estimated directly from the buoyancy frequency and those inferred from the fits of the analytical expression to the period spacings for the two cases studied here are smaller than 7%, for all parameters, but the amplitudes. For the step-like glitch, the amplitude value estimated from the buoyancy frequency is 11% larger than the median of the distribution inferred from the fit to the period spacings. However, Fig. 1b reassures us that the glitch amplitude is adequately recovered when considering the uncertainty introduced by the adopted step-function model. In the case of the glitch modelled by a Gaussian, the inferred amplitude is found to be about 60% larger than expected. This difference is likely related to our inability to correctly model the eigenfunction inside the glitch, where the asymptotic analysis fails. Further tests shall be performed in future work covering a larger set of models, to calibrate the inferred amplitude against the true one and establish the range of applicability of the expression in the case of the Gaussian-like glitch.

In addition, we find that the analytical expression describing the period spacing for mixed modes propagating in the presence of a buoyancy glitch represents well the period spacing derived numerically for a red-giant model exhibiting such a glitch. However, our results indicate that in the case considered here, of a RGB star at the luminosity bump, the fit of the analytical expression to the model period spacing based on a global χ^2 minimisation criteria does not allow us to constrain the glitch parameters. This is because the period spacing variations are dominated by the effect of the mode coupling. Alternative approaches to fit the analytical expression to model data that may allow to highlight the impact of the glitch on the oscillation periods and, thus, constrain the glitch parameters, are being considered and will be discussed in a future work.

Finally, our fit of the analytical expression to mixed-mode model data in the absence of buoyancy glitches indicates a clear frequency dependence of the coupling coefficient q . This depend-

ance, which is theoretically expected for stars with v_{\max} smaller than $\sim 100\mu\text{Hz}$, may need to be considered when fitting data of intermediate to high luminosity red-giant stars, depending on the number of radial orders observed.

Interestingly, our results also show that by fitting the proposed analytical expression to the dipole mixed-mode period spacing, it might be possible to extract the frequencies of the pure acoustic dipole modes that would exist, had these modes not been mixed in red-giant stars.

ACKNOWLEDGEMENTS

We thank the referee, Sébastien Deheuvels, for making very pertinent comments on the first version of this manuscript. We also thank Stefano Garcia for useful comments and for providing a modified RGB model with a glitch of higher amplitude to test the results of Appendix A under different conditions. This work was supported by FCT - Fundação para a Ciência e a Tecnologia through national funds and by FEDER through COMPETE2020 - Programa Operacional Competitividade e Internacionalização by these grants: UID/FIS/04434/2013 & POCI-01-0145-FEDER-007672, PTDC/FIS-AST/30389/2017 & POCI-01-0145-FEDER-030389. Funding for the Stellar Astrophysics Centre is provided by The Danish National Research Foundation (Grant DNRF106). The research was supported by the ASTERISK project (ASTERoseismic Investigations with SONG and Kepler) funded by the European Research Council (Grant agreement no.: 267864). D.S is the recipient of an Australian Research Council Future Fellowship (project number FT1400147).

References

- Aerts C., Christensen-Dalsgaard J., Kurtz D. W., 2010, *Asteroseismology*
- Aerts C., Mathis S., Rogers T., 2018, arXiv e-prints,
- Baglin A., Auvergne M., Barge P., Deleuil M., Catala C., Michel E., Weiss W., COROT Team 2006, in Fridlund M., Baglin A., Lochard J., Conroy L., eds, *ESA Special Publication Vol. 1306, The CoRoT Mission Pre-Launch Status - Stellar Seismology and Planet Finding*, p. 33
- Bossini D., et al., 2015, *MNRAS*, **453**, 2290
- Brassard P., Fontaine G., Wesemael F., Hansen C. J., 1992, *ApJS*, **80**, 369
- Broomhall A.-M., et al., 2014, *MNRAS*, **440**, 1828
- Brown T. M., 1991, *ApJ*, **371**, 396
- Christensen-Dalsgaard J., 2008a, *Ap&SS*, **316**, 13
- Christensen-Dalsgaard J., 2008b, *Ap&SS*, **316**, 113
- Christensen-Dalsgaard J., 2012, in Shibahashi H., Takata M., Lynas-Gray A. E., eds, *Astronomical Society of the Pacific Conference Series Vol. 462, Progress in Solar/Stellar Physics with Helio- and Asteroseismology*, p. 503 ([arXiv:1110.5012](https://arxiv.org/abs/1110.5012))
- Christensen-Dalsgaard J., et al., 1996, *Science*, **272**, 1286
- Constantino T., Campbell S. W., Christensen-Dalsgaard J., Lattanzio J. C., Stello D., 2015, *MNRAS*, **452**, 123
- Cunha M. S., Stello D., Avelino P. P., Christensen-Dalsgaard J., Townsend R. H. D., 2015, *ApJ*, **805**, 127
- Deheuvels S., Ballot J., Beck P. G., Mosser B., Østensen R., García R. A., Goupil M. J., 2015, *A&A*, **580**, A96
- Foreman-Mackey D., Hogg D. W., Lang D., Goodman J., 2013, *PASP*, **125**, 306
- Gilliland R. L., et al., 2010, *PASP*, **122**, 131
- Gough D. O., 1993, in Zahn J.-P., Zinn-Justin J., eds, *Astrophysical Fluid Dynamics - Les Houches 1987*, pp 399–560
- Gough D. O., 2002, in Battrick B., Favata F., Roxburgh I. W., Galadi D., eds, *ESA Special Publication Vol. 485, Stellar Structure and Habitable Planet Finding*, pp 65–73

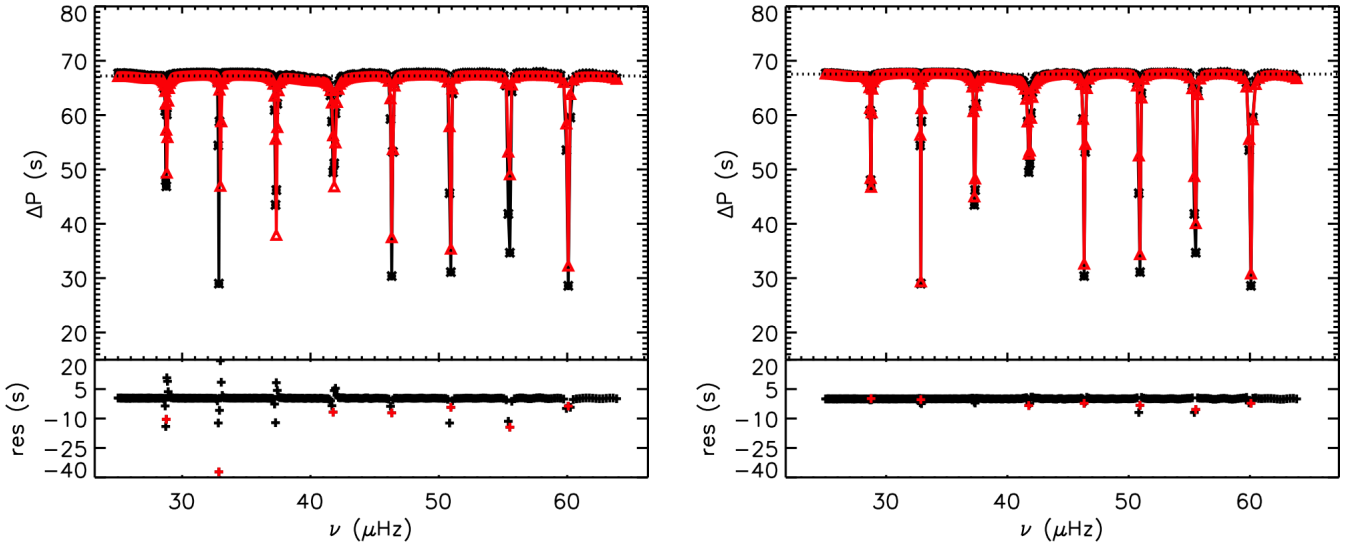


Figure 9. Top panels: comparison between the period spacing derived from ADIPLS for our RGB-2 model (with a core glitch) (black line and asterisks) with that obtained from Eqs (24)-(26) with the most likely parameters from our fit, performed in the frequency range shown in the figure (red line and triangles). Left is for $\omega_{a,n}$ derived from Eq. (20) and right for $\omega_{a,n}$ left as free parameters in the fit. Moreover, q was taken to depend linearly on the frequency, according to eq. (21) and the glitch parameters were fixed from the outset, based on the results of section 3. Bottom panels: the residuals (‘ADIPLS period spacing’ – ‘analytical period spacing’). The red symbols mark the residuals at the minima of the ADIPLS period spacings.

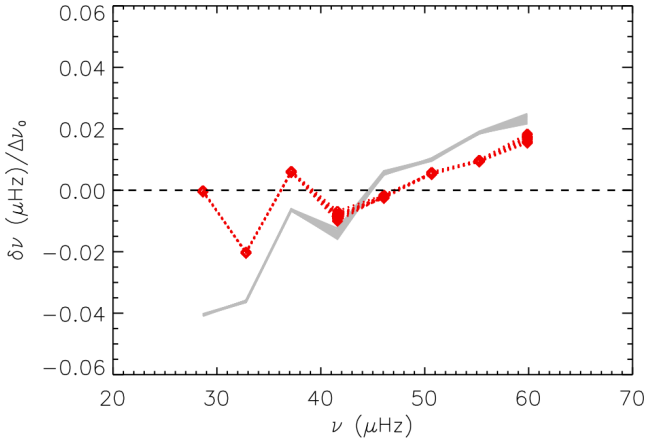


Figure 10. Difference between the pure acoustic frequencies $\nu_{a,n} = \omega_{a,n}/2\pi$ estimated from fitting Eqs (24)-(26) to the model period spacings with $\omega_{a,n}$ taken as free parameters and those estimated from otherwise similar fits but with $\omega_{a,n}$ given by: i) Eq. (19) (grey curve) and ii) Eq. (20) (red-dashed curve; diamonds). The difference is scaled by the large frequency separation and is shown for a sample of 30 best fitted models (with similar likelihood), whose superposition is reflected in the slight broadening of the lines plotted.

[A&A, 584, A50](#)

Mosser B., Gehan C., Belkacem K., Samadi R., Michel E., Goupil M.-J.,

2018, [A&A, 618, A109](#)

Pedersen M. G., Aerts C., Pápics P. I., Rogers T. M., 2018, preprint, ([arXiv:1802.02051](#))

Shibahashi H., 1979, *PASJ*, **31**, 87

Takata M., 2016, *PASJ*, **68**, 109

Tassoul M., 1980, *ApJS*, **43**, 469

Unno W., Osaki Y., Ando H., Saio H., Shibahashi H., 1989, Nonradial oscillations of stars

Wu T., Li Y., Deng Z.-m., 2018, *ApJ*, **867**, 47

Gough D. O., 2007, *Astronomische Nachrichten*, **328**, 273

Goupil M. J., Mosser B., Marques J. P., Ouazzani R. M., Belkacem K., Lebreton Y., Samadi R., 2013, [A&A, 549, A75](#)

Hekker S., Christensen-Dalsgaard J., 2017, *A&ARv*, **25**, 1

Hekker S., Elsworth Y., Angelou G. C., 2018, [A&A, 610, A80](#)

Houdek G., Gough D. O., 2007, *MNRAS*, **375**, 861

Jiang C., Christensen-Dalsgaard J., 2014, *MNRAS*, **444**, 3622

Kjeldsen H., Bedding T. R., 1995, *A&A*, **293**, 87

Miglio A., Montalbán J., Noels A., Eggenberger P., 2008, *MNRAS*, **386**, 1487

Monteiro M. J. P. F. G., Christensen-Dalsgaard J., Thompson M. J., 1994, *A&A*, **283**, 247

Mosser B., et al., 2012, [A&A, 540, A143](#)

Mosser B., Vrad M., Belkacem K., Deheuvels S., Goupil M. J., 2015,

APPENDIX A: SIGNATURE OF BUOYANCY GLITCHES

The signature on the period spacing from a buoyancy glitch modelled by a Dirac delta function has been derived by Cunha et al. (2015) based on the variable $\Psi = (r^3/g\rho\tilde{f})^{1/2}\delta p$, where δp is the Lagrangian pressure perturbation and \tilde{f} is a function of frequency and of the equilibrium structure (the f-mode discriminant defined by equation (35) of Gough (2007)). Here we present similar derivations for the cases of buoyancy glitches modelled by a step function and by a Gaussian function, respectively.

The starting point is the wave equation,

$$\frac{d^2\Psi}{dr^2} + K^2\Psi = 0, \quad (\text{A1})$$

derived from the linear, adiabatic pulsation equations, for the case of a spherically symmetric equilibrium under the Cowling approximation. The radial wavenumber K is defined by,

$$K^2 = \frac{\omega^2 - \omega_c^2}{c^2} - \frac{L^2}{r^2} \left(1 - \frac{\mathcal{N}^2}{\omega^2} \right), \quad (\text{A2})$$

where ω_c and \mathcal{N} are generalisations of the usual critical acoustic frequency and buoyancy frequency, respectively, which account for all terms resulting from the spherical geometry of the problem. The exact forms of these quantities can be found in equations (5.4.8) and (5.4.9) of Gough (1993). In practice \mathcal{N} is very similar to N throughout the wave propagation cavity, where it will be relevant for our analysis, and, thus, we approximate the former by the latter from the outset, similar to what has been done in Cunha et al. (2015).

A1 Impact on pure gravity modes

In short, the derivation of the signature on the period spacing from the buoyancy glitch is performed by considering the asymptotic solutions to Eq. (A1) on each side of the glitch and applying appropriate matching conditions at the glitch location. We recall that the asymptotic solutions well inside the g-mode cavity, inwards and outwards from the glitch position are, respectively

$$\Psi_{\text{in}} \sim \tilde{\Psi}_{\text{in}} K_{\text{in}}^{-1/2} \sin \left(\int_{r_1}^r K_{\text{in}} dr + \frac{\pi}{4} \right), \quad (\text{A3})$$

and

$$\Psi_{\text{out}} \sim \tilde{\Psi}_{\text{out}} K_{\text{out}}^{-1/2} \sin \left(\int_r^{r_2} K_{\text{out}} dr + \frac{\pi}{4} \right), \quad (\text{A4})$$

where $\tilde{\Psi}_{\text{in}}$ and $\tilde{\Psi}_{\text{out}}$ are constants and K_{in} and K_{out} refer to K computed from N_{in} and N_{out} , respectively.

Glitch modelled by a step function

In the case of the glitch modelled by the step-like function, the discontinuity in the buoyancy frequency at $r = r^*$ leads to a discontinuity in the wavenumber at the same position. Well inside the g-mode cavity, $K \approx \frac{LN}{\omega r}$ and, thus, the relative amplitude of the discontinuity in the wavenumber is given by,

$$\frac{\Delta K}{K_{\text{out}}^*} \approx \frac{N_{\text{in}}^*}{N_{\text{out}}^*} - 1 = A_{\text{st}}, \quad (\text{A5})$$

where $\Delta K = K_{\text{in}}|_{r \rightarrow r_-^*} - K_{\text{out}}|_{r \rightarrow r_+^*}$ and the subscript \star indicates that the quantities are to be taken at $r \rightarrow r_{\pm}^*$.

Similarly to the case of the glitch modelled by the Dirac delta

function, we impose the continuity of Ψ at $r = r^*$ ⁸. Moreover, by integrating the wave equation (A1) once across the glitch, letting the width of the region where the integration is performed tend to zero, it becomes evident that the derivative of Ψ must also be continuous at $r = r^*$, unlike what was found in the case of the glitch modelled by the Dirac delta function. This is because the integral of the step function is a continuous function, while the integral of a Dirac delta function is not.

Imposing that both Ψ and its derivative, taken asymptotically, are continuous at the glitch position, we find,

$$\begin{aligned} & \sin \left(\int_{r_1}^{r_2} K dr + \frac{\pi}{2} \right) = \\ & -A_{\text{st}} \sin \left(\int_{r^*}^{r_2} K_{\text{out}} dr + \frac{\pi}{4} \right) \cos \left(\int_{r_1}^{r^*} K_{\text{in}} dr + \frac{\pi}{4} \right). \end{aligned} \quad (\text{A6})$$

Equation (A6) provides the eigenvalue condition in the presence of a glitch modelled by a step-like function. It differs in two main aspects from the condition derived by Cunha et al. (2015) for the glitch modelled by a Dirac delta function (their equation 13). Firstly, the amplitude multiplying the sinusoidal functions on the rhs is independent of frequency, implying that the amplitude of the signature of the glitch on the period spacing will also be independent of the frequency in this case. Secondly, the rhs does not remain invariant when the arguments inside the sinusoidal functions are interchanged, highlighting the fact that in the present case glitches positioned symmetrically about the center of the cavity produce different signatures.

Next, we consider the specific case of a glitch located in the inner half of the propagation cavity, *i.e.* $\tilde{\omega}_g^*/\omega_g < 0.5$. Writing,

$$\int_{r^*}^{r_2} K_{\text{out}} dr + \frac{\pi}{4} = \int_{r_1}^{r_2} K dr + \frac{\pi}{2} - \int_{r_1}^{r^*} K_{\text{in}} dr - \frac{\pi}{4}, \quad (\text{A7})$$

and substituting in Eq. (A6) we find,

$$\sin \left(\int_{r_1}^{r_2} K dr + \frac{\pi}{2} + \Phi \right) = 0, \quad (\text{A8})$$

where Φ , and a new quantity, B , are defined by the following system of equations,

$$\begin{cases} B \cos \Phi &= 1 + A_{\text{st}} \cos^2 \left(\int_{r_1}^{r^*} K_{\text{in}} dr + \pi/4 \right) \\ B \sin \Phi &= -\frac{1}{2} A_{\text{st}} \cos \left(2 \int_{r_1}^{r^*} K_{\text{in}} dr \right) \end{cases} \quad (\text{A9})$$

Finally, to relate the phase Φ to the parameters characterising the glitch, we approximate the integral in the arguments of the sinusoidal functions in Eq. (A9) by $\int_{r_1}^{r^*} K_{\text{in}} dr \approx \int_{r_1}^{r^*} \frac{LN}{\omega r} dr + \delta \equiv \frac{\tilde{\omega}_g^*}{\omega} + \delta$. This approximation follows from approximating K by $\frac{LN}{\omega r}$ inside the cavity. Because near the turning point, r_1 , the wavenumber approaches zero, this approximation leads to a slight overestimation of the value of the wavenumber integral which is compensated by the introduction of the phase δ . The phase δ is, thus, related to the details of mode reflection near the turning points of the propagation cavity, more specifically, in the present case near the inner turning point.

The phase Φ defined by Eq. (A9), with the approximation described above, is then differentiated and used in Eq. (6) to derive the analytical expression for the period spacing given by Eq. (14).

⁸ Strictly speaking, the continuity condition is satisfied by δp . However, we have verified from the numerical solutions computed with ADIPLS that this condition is also very closely satisfied by Ψ .

Glitch modelled by a Gaussian function

In the case of the glitch modelled by the Gaussian-like function, the variation in the buoyancy frequency around $r = r^*$ produces a variation in the wavenumber that can be expressed by

$$\frac{\Delta K}{K_0} \approx \frac{A_G}{\sqrt{2\pi}\Delta_g} \exp\left(-\frac{(\omega_g^r - \omega_g^*)^2}{2\Delta_g^2}\right), \quad (\text{A10})$$

where, as before, we have assumed the glitch is located well inside the g-mode cavity and, thus, approximated the wave number by $K \approx \frac{LN}{\omega r}$, and defined the unperturbed wavenumber as $K_0 \approx \frac{LN_0}{\omega r}$.

Similarly to what was done in previous cases, to establish the eigenvalue condition for this case, we need to match the asymptotic solutions given by Eqs (A3)-(A4) and their derivatives across the glitch. We note, however, that unlike the cases of glitches modelled by a Dirac delta function and by a step-like function, here the glitch is not infinitely thin. Therefore, the exact matching would require that we establish first how the eigenfunctions are perturbed inside the glitch, which is unknown within the framework of our study, because the solutions that we are employing were derived asymptotically (hence, neglecting small-scale perturbations to the background).

To proceed, we therefore make a significant simplification to the problem which consists in assuming that the eigenfunction inside the glitch has the same functional form as that derived asymptotically in the absence of a glitch, with a slowly varying amplitude and a rapidly varying oscillatory part. In practice, this is achieved by extending the solutions on both sides of the glitch all the way to $r = r^*$, keeping the amplitude proportional to the unperturbed $K_0^{-1/2}$. Under this assumption, the continuity of Ψ at $r = r^*$ imposes that

$$\tilde{\Psi}_{\text{in}} = \frac{\sin\left(\int_{r_1}^{r^*} K dr + \frac{\pi}{4}\right)}{\sin\left(\int_{r_1}^{r^*} K dr + \frac{\pi}{4}\right)} \tilde{\Psi}_{\text{out}}, \quad (\text{A11})$$

where K_{in} and K_{out} were assumed equal to K on each side of r^* , and the integration of the wave equation (A1) across the glitch gives,

$$\left[\frac{d\Psi_{\text{out}}}{dr} - \frac{d\Psi_{\text{in}}}{dr}\right]_{r^*} = -\int_{r^*-\Delta r}^{r^*+\Delta r} \Delta K \Psi K dr, \quad (\text{A12})$$

where $\pm\Delta r$ defines the region of impact of the glitch.

Equation (A12) shows that under our assumption the integrated impact of the glitch on the phase of the wave is taken at a single position, namely $r = r^*$. To compute the integral on the rhs of Eq. (A12) we need again to consider the eigenfunction inside the glitch. For mathematical consistency, we should take the extended solutions on each side of r^* . However, in the actual problem the phase does not jump at a single position. Thus, using the solution that incorporates that phase jump in the computation of the phase jump itself, is not necessarily a better approximation than adopting a solution that does not incorporate a phase jump at r^* , as would be achieved by taking the inner or the outer solution throughout the whole glitch. Given the above, we derive the eigenvalue conditions for both cases, and test their performance a posteriori through the comparison with the numerical results. That comparison allows us also to check the implications of the simplification introduced in this analysis.

Adopting the extended solutions on each side of the glitch, and combining Eqs (A11)-(A12), we find, after some algebra, the eigenvalue condition,

$$\sin\left(\int_{r_1}^{r^*} K dr + \frac{\pi}{2}\right) \left(1 + \frac{A_G \alpha}{\omega}\right) =$$

$$A_G f_{\omega}^{\Delta_g} \sin\left(\int_{r_1}^{r^*} K dr + \frac{\pi}{4}\right) \sin\left(\int_{r^*}^{r_2} K dr + \frac{\pi}{4}\right), \quad (\text{A13})$$

where $\alpha = 0.5 \omega f_{\omega}^{\Delta_g} \text{erfi}(a)$, with $a = \sqrt{0.5} \Delta_g \omega^{-1}$, $f_{\omega}^{\Delta_g} = \omega^{-1} e^{-a^2}$, and erfi is the imaginary error function.

However, if we adopt either the extended inner solution or the extended outer solution throughout the whole integral, we find,

$$\sin\left(\int_{r_1}^{r_2} K dr + \frac{\pi}{2}\right) = A_G f_{\omega}^{\Delta_g} \sin\left(\int_{r_1}^{r^*} K dr + \frac{\pi}{4}\right) \sin\left(\int_{r^*}^{r_2} K dr + \frac{\pi}{4}\right). \quad (\text{A14})$$

Equation (A13) differs from Eq. (A14) due to the presence of the term $A_G \alpha / \omega$ on the lhs. While α is always smaller than ~ 0.3 , A_G / ω may be large, as no assumption is made about the strength of the glitch. In that case, the two eigenvalue conditions will differ significantly. As we shall see, that difference will have an impact on the amplitude recovered when fitting the analytical period spacing derived for each case to the numerical one.

We note that both Eq. (A13) and (A14) predict that the amplitude of the glitch signature is frequency dependent. This is unlike what was found for the step-like glitch (cf. Eq. (A6)). Moreover, in both cases we can note that the rhs remains invariant when the arguments inside the sinusoidal functions on the rhs are interchanged, highlighting that glitches modelled by a Gaussian function positioned symmetrically about the centre of the cavity produce similar signatures on pure gravity waves. In reality, the requirement that the wave solutions are regular at the centre of the star is expected to introduce a slight asymmetry between the boundary conditions on the left and right sides of the g-mode cavity, leading to a slight asymmetry also in the glitch signature. That, however, is not accounted for in the asymptotic analysis presented here and shall be subject to further discussion in future work.

Next, we consider the specific case of a glitch located in the outer half of the propagation cavity, i.e. $\omega_g^* / \omega_g < 0.5$. Writing

$$\int_{r_1}^{r^*} K dr + \frac{\pi}{4} = \int_{r_1}^{r^*} K dr + \frac{\pi}{2} - \int_{r^*}^{r_2} K dr - \frac{\pi}{4}, \quad (\text{A15})$$

and substituting in Eqs (A13) and (A14) we find

$$\sin\left(\int_{r_1}^{r^*} K dr + \frac{\pi}{2} + \Phi\right) = 0, \quad (\text{A16})$$

where, Φ and B take different forms, depending on the eigenvalue condition adopted. For the eigenvalue condition defined by (A13) we find

$$\begin{cases} B \cos \Phi &= 1 + \frac{A_G \alpha}{\omega} - \frac{1}{2} A_G f_{\omega}^{\Delta_g} \cos\left(2 \int_{r^*}^{r_2} K dr\right) \\ B \sin \Phi &= A_G f_{\omega}^{\Delta_g} \sin^2\left(\int_{r^*}^{r_2} K dr + \frac{\pi}{4}\right) \end{cases} \quad (\text{A17})$$

while for the eigenvalue condition defined by (A14) Φ and B take the form

$$\begin{cases} B \cos \Phi &= 1 - \frac{1}{2} A_G f_{\omega}^{\Delta_g} \cos\left(2 \int_{r^*}^{r_2} K dr\right) \\ B \sin \Phi &= A_G f_{\omega}^{\Delta_g} \sin^2\left(\int_{r^*}^{r_2} K dr + \frac{\pi}{4}\right) \end{cases} \quad (\text{A18})$$

To relate Φ to the parameters characterising the glitch we approximate $\int_{r^*}^{r_2} K dr \approx \int_{r^*}^{r_2} \frac{LN}{\omega r} dr + \delta \equiv \frac{\omega_g^*}{\omega} + \delta$, where in this case the phase δ is related to the details of the mode reflection near the outer turning point.

When the phase Φ , with the approximation above, is differentiated and used in Eq. (6), the period spacing becomes

$$\frac{\Delta P}{\Delta P_{\text{as}}} \approx [1 - \mathcal{F}_G]^{-1}, \quad (\text{A19})$$

where \mathcal{F}_G takes different forms, depending on whether we use Eqs (A17) or Eqs (A18). If Φ and B are defined by Eqs (A17), we find

$$\mathcal{F}_G = -\frac{A_G f_{\omega}^{\Delta_g}}{B^2} \frac{\omega_g^*}{\omega_g} \left\{ \left(1 + \frac{A_G \alpha}{\omega} \right) \cos \beta_1 + \left(-\frac{\omega}{\omega_g^*} \frac{d \ln f_{\omega}^{\Delta_g}}{d \ln \omega} - A_G f_{\omega}^{\Delta_g} - \frac{A_G a}{\sqrt{\pi} \omega_g^*} \right) \sin^2 \beta_2 \right\} \quad (\text{A20})$$

with $\beta_1 = 2\omega_g^*/\omega + 2\delta$, and $\beta_2 = \omega_g^*/\omega + \pi/4 + \delta$. If, however, Φ and B are defined by Eqs (A18), we find

$$\mathcal{F}_G = -\frac{A_G f_{\omega}^{\Delta_g}}{B^2} \frac{\omega_g^*}{\omega_g} \left[\cos \beta_1 + \left(-\frac{\omega}{\omega_g^*} \frac{d \ln f_{\omega}^{\Delta_g}}{d \ln \omega} - A_G f_{\omega}^{\Delta_g} \right) \sin^2 \beta_2 \right] \quad (\text{A21})$$

Given the symmetry of the eigenvalue condition discussed before, the same expressions for the period spacing would be found if the glitch had been located in the inner half of the propagating cavity, but with ω_g^* replaced by $\tilde{\omega}_g^*$.

The analytical expressions provided by Eqs (A20) and (A21) have been tested against the period spacing derived directly from the numerical solutions to the pulsation equations in the absence of coupling between p and g modes, which were computed with ASTER, for our RGB-2 model. The results are shown in Table A1, where we confront the glitch parameters inferred from the fit of each expression to the numerical results and those measured directly from inspection of the buoyancy frequency.

While the analytical expressions given by Eqs (A20) and (A21) provide a good fit to the numerical data (with a likelihood comparable to the fit illustrated in Fig. 5), both the amplitude and the width of the glitch inferred from the fit are about twice the estimated value. To understand the origin of that, we recall that the main impact expected from the width of the Gaussian glitch is an attenuation of the glitch signature with decreasing frequency, resulting from the fact that the local wavenumber approaches the characteristic scale of the glitch, as the frequency decreases. It, thus, seems quite likely that the simplification introduced in the analysis presented here, namely, accounting only for the integrated effect of the glitch on the phase of the wave, is responsible for the differences seen in the numerical and analytical period spacings.

Since the asymptotic approach adopted here precludes us from fully taking into account the finite width of the glitch, it is important to compare the results from our simplified approach with those derived in the limit case of a small glitch, for which we can derive the impact of the glitch on the frequencies, to first order, without knowledge of the perturbed eigenfunctions. We note that in this limit the eigenvalue condition expressed by Eq. (A13) approaches that given by Eq. (A14) because A/ω is small. That analysis has, in fact, been carried out in previous works for the case of a Gaussian-like acoustic glitch associated to the helium second ionisation zone (Gough 2002; Houdek & Gough 2007). Those authors studied the impact of that glitch on the p modes and found an exponential decrease of the amplitude of the glitch signature with the square of the frequency⁹, but with a factor of 4 greater than the one found in the current analysis. Indeed, following their analysis, we recover

⁹ We note that because the authors analysed the impact of an acoustic glitch on the p modes the dependence on frequency they found is, as expected, inverse to what is found here. While we find an exponential decrease with decreasing frequency squared, they find an exponential decrease with increasing frequency squared.

the analytical expression for the period spacing given by Eq. (A21) if the function $f_{\omega}^{\Delta_g}$ is replaced by $f_{\omega}^{\Delta_g} = \omega^{-1} e^{-4a^2}$.

Motivated by that limit result, which should be satisfied by the more general expression, we have multiplied the exponent of the function $f_{\omega}^{\Delta_g}$ by a factor of 4 and performed new fits. With this modification, the glitch width inferred from the fit of both analytical expressions to the numerical period spacings is brought into agreement with the value estimated directly from the buoyancy frequency, as seen from the two last rows of Table A1. The amplitudes, on the other hand, are hardly changed by the modification introduced. We, thus, find that both modified analytical expressions provide a good representation of the data (as illustrated in Fig. 5, for the case of Eq. (A21) with the modified $f_{\omega}^{\Delta_g}$), but both lead to an overestimation of the amplitude of the glitch. We have tested the two modified expressions on an otherwise similar model, but with a glitch with an amplitude about three times larger. We found results very similar to those found for the model discussed here, where the position and width of the glitch are adequately recovered, but the amplitude is overestimated by the same factor as before (~ 1.5) in the case of Eq. (A21) and by a larger factor in the case of Eq. (A20). The fact that Eq. (A20) is more complex than Eq. (A21) and results in a larger overestimation of the glitch amplitude, leads us to the conclusion that Eq. (A21) with the modified $f_{\omega}^{\Delta_g}$ provides the best of the four options discussed here to fit the model data.

A2 Impact on mixed modes

To combine the effect of mode coupling with that of a glitch modelled by a Gaussian function, we follow again the analysis performed in Cunha et al. (2015) for the Dirac-delta glitch. When the waves propagate also in the p-mode cavity, Eq. (A4) is substituted by

$$\Psi_{\text{out}} \sim \tilde{\Psi}_{\text{out}} K_{\text{out}}^{-1/2} \sin \left(\int_r^{r_2} K_{\text{out}} dr + \frac{\pi}{4} + \varphi \right), \quad (\text{A22})$$

where, as for the case of the Gaussian-like glitch without mode-coupling, this solution on the rhs of the glitch shall be extended all the way to $r = r^*$, keeping the amplitude proportional to $K_0^{-1/2}$. The frequency-dependent coupling phase φ is defined by Eq. (7) and expresses the influence of the p-mode cavity on the wave solution.

For the specific case of a glitch located in the outer half of the propagation cavity, as is our RGB-2 model, it follows that the eigenvalue condition can be expressed as

$$\sin \left(\int_{r_1}^{r_2} K dr + \frac{\pi}{2} + \Phi + \varphi \right) = 0, \quad (\text{A23})$$

where, following the conclusions of Sec. A1, now Φ and B are defined by the following system of equations

$$\begin{cases} B \cos \Phi &= 1 - \frac{1}{2} A_G f_{\omega}^{\Delta_g} \cos \left(2 \int_{r_*}^{r_2} K dr + 2\varphi \right) \\ B \sin \Phi &= A_G f_{\omega}^{\Delta_g} \sin^2 \left(\int_{r_*}^{r_2} K dr + \frac{\pi}{4} + \varphi \right), \end{cases} \quad (\text{A24})$$

Here, as before, the function f is formally derived to be $f_{\omega}^{\Delta_g} = \omega^{-1} e^{-a^2} \equiv \omega^{-1} e^{-\frac{1}{2} \Delta_g^2 \omega^{-2}}$, but for the reasons discussed in Sections 3 and A1 for the case of a Gaussian-like glitch and no coupling, it will be replaced by $f_{\omega}^{\Delta_g} = \omega^{-1} e^{-2\Delta_g^2 \omega^{-2}}$ motivated by the low-amplitude glitch limit and the numerical results.

Approximating, $\int_{r_*}^{r_2} K dr \approx \int_{r_*}^{r_2} \frac{LN}{\omega r} dr + \delta$ in Eqs (A24), differentiating Φ , and substituting it in Eq. (6), we finally find the period spacing given by Eqs (24)-(26).

Table A1. Second and third rows: parameters derived from the fit of the analytical expressions given by Eqs (A20) and (A21) to the period spacing derived from ASTER for the RGB-2 model (at the luminosity bump). Fourth and fifth rows: the same as the preceding rows, but with the function $f_{\omega}^{\Delta g}$ in the analytical expressions replaced by $f_{\omega}^{\Delta g} = \omega^{-1} e^{-4a^2}$. The values shown correspond to the best fit model. For comparison, the values of the glitch parameters estimated directly from the buoyancy frequency obtained with ASTEC (Fig. 1 d) are also shown on the last row.

	A_G (10^{-6} rad/s)	ω_g^* (10^{-6} rad/s)	Δ_g (10^{-6} rad/s)
Eq (A20)	898	1763	255
Eq (A21)	602	1747	315
Eq (A20); modified $f_{\omega}^{\Delta g}$	803	1754	155
Eq (A21); modified $f_{\omega}^{\Delta g}$	608	1748	159
Estimated	380	1632	156

Finally, we note that unlike in the case of the pure gravity modes, the signature on the mixed modes from the Gaussian-like glitch is not invariant to symmetric changes of the glitch about the center of the g-mode cavity. The reason is that the conditions on the left and right of the glitch are not the same, as a result of the p-mode cavity. Mathematically, that is seen from the comparison of Eq. (A3) with Eq. (A4) and Eq. (A22), respectively. While the first two are identical when considering equivalent buoyancy distances from each extreme of the cavity, the same is not true when the first and last of these equations are considered.

APPENDIX B: ESTIMATING THE PURELY ACOUSTIC DIPOLE-MODE FREQUENCIES

In a red-giant star, the modes of degree $l = 1$ have a mixed nature. Hence, their frequencies are different from those that pure acoustic modes would have in the same star. Nevertheless, knowledge of those pure acoustic frequencies, $\omega_{a,n}$, may be necessary to apply the analytic expressions provided in this work for the period spacing in the presence of mode coupling. One possible way to estimate those frequencies is to start from the frequencies of radial modes, which are also observed in red giants and are always purely acoustic. In Section 4 we proposed two expressions to estimate the frequencies $\omega_{a,n}$. Here, we use the same expressions to estimate the frequencies of $l = 1$ modes in a solar model. Because in the sun $l = 1$ modes are purely acoustic, by doing so we can check the performance of each expression against the known purely acoustic model frequencies.

Inspired in the results of the asymptotic analysis (Tassoul 1980), we write the frequencies of high radial-order purely acoustic modes in the following form,

$$v_{n,l} \approx \left(n + \frac{l}{2}\right) \Delta v_0 - \frac{AL^2 \Delta v_0^2}{v_{n,l}} + G(v_{n,l}), \quad (\text{B1})$$

where A is sensitive to the conditions in the innermost layers of the star and $G(v_{n,l})$ is a function of frequency that accounts for near surface effects considered, e.g., in the asymptotic analysis by Gough (1993), and also for deviations from the asymptotically-derived frequencies introduced, e.g., by the presence of acoustic glitches located inside the p-mode cavity. The important aspect to retain is that these frequency-dependent effects are present both when considering $l = 0$ and $l = 1$ modes. At the radial mode frequencies, the function G reduces to $G(v_{n,0}) \approx v_{n,0} - n\Delta v_0$.

Considering that the function $G(v_{n,l})$ may vary slowly with

frequency (meaning, on a scale of many radial orders), we can consider, first, the following rough approximation for the frequencies of the $l = 1$ modes,

$$v_{n,1} \approx v_{n,0} + \frac{1}{2} \Delta v_0 + \frac{C}{(v_{n,0} + 1/2 \Delta v_0)}, \quad (\text{B2})$$

where $C = -AL^2 \Delta v_0^2$. Expressing the above in terms of angular frequencies, we find the option adopted in Eq. (19).

Alternatively, we may try to account for the fact that, for a given radial order, the function $G(v_{n,l})$ will take slightly different values if considered at the frequency of the radial mode or at the frequency of the dipole mode. That can in principle be done by interpolating the function G derived from the radial modes, at the frequencies estimated for the dipole modes. If G were indeed a slowly varying function of frequency, one could consider fitting it simultaneously across a number of $l = 0$ radial orders prior to interpolating it. However, one of the contributions to G comes from the acoustic glitches mentioned before, which may introduce significant variations across just a few radial orders. For that reason, after trying several fitting plus interpolation options we concluded that the approach yielding the best results consists on linearly interpolating G between each two consecutive radial mode frequencies taking its value at $v_{n,0} + 1/2 \Delta v_0$, which is the first-order estimate of the dipolar mode frequencies. This option, applied to Eq. (B1), leads us to the following estimate of the dipole-mode acoustic frequencies:

$$v_{n,1} \approx \left(n + \frac{1}{2}\right) \Delta v_0 + \frac{C}{(v_{n,0} + 1/2 \Delta v_0)} + G(v_{n,0} + 1/2 \Delta v_0), \quad (\text{B3})$$

where the last term on the rhs is to be interpreted as the value of the function G obtained from interpolation at the frequencies defined by the expression within the brackets. This estimate, expressed in terms of angular frequencies, provides the option adopted in Eq. (20).

The comparison between the model S dipole-mode frequencies, computed with ADIPLS, and the estimates proposed by Eqs (B2) and (B3), corresponding to the options 1. and 2., respectively, in Sec. 4, is shown in Fig B1. As expected, Eq. (B3) (option 2. in Sec. 4) represents more closely the true model S dipole-mode frequencies. The differences that are still found when that option is considered stem from the fact that acoustic glitches introduce frequency variations that are not fully accounted for by the linear interpolation between radial modes considered here.

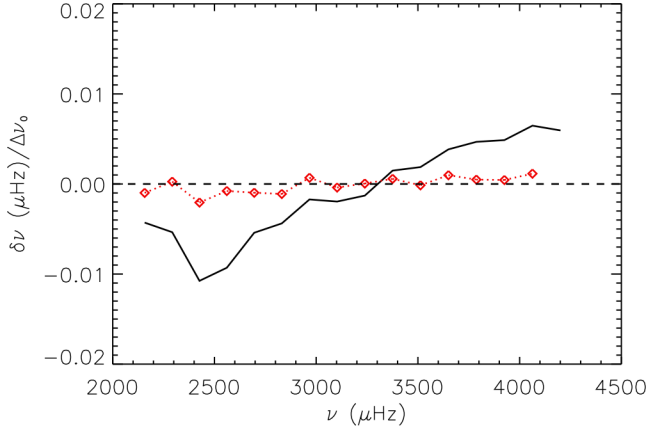


Figure B1. Difference between the $l = 1$ acoustic frequencies, $\nu_{n,1}$, computed with ADIPLS for the solar model S (Christensen-Dalsgaard et al. 1996) and those estimated from: i) Eq. (B2) (grey curve) and ii) Eq. (B3) (red-dashed curve; diamonds). The difference is scaled by the average solar large frequency separation computed from the $l = 0$ modes within the range of radial orders shown, namely $13 \leq n \leq 28$. In this case the constant $C = -AL^2\Delta\nu_0^2$ was estimated through uniformly weighted averages over the same range of n , $\langle (\nu_{n,1} - \nu_{n,0} - 0.5\Delta\nu_0)(\nu_{n,0} + 0.5\Delta\nu_0) \rangle$ and $\langle (\nu_{n,1} - (n + 0.5)\Delta\nu_0 - G(\nu_{n,0} + 0.5\Delta\nu_0))(\nu_{n,0} + 0.5\Delta\nu_0) \rangle$, respectively.

This paper has been typeset from a \LaTeX file prepared by the author.